



## City Research Online

### City, University of London Institutional Repository

---

**Citation:** Qian, K., Weng, Y., Fu, F. & Deng, X. (2020). Numerical Evaluation of the Reliability of Using Single-Story Substructures to Study Progressive Collapse Behaviour of Multi-Story RC Frames. *Journal of Building Engineering*, 33, 101636. doi: 10.1016/j.jobe.2020.101636

This is the accepted version of the paper.

This version of the publication may differ from the final published version.

---

**Permanent repository link:** <https://openaccess.city.ac.uk/id/eprint/24416/>

**Link to published version:** <https://doi.org/10.1016/j.jobe.2020.101636>

**Copyright:** City Research Online aims to make research outputs of City, University of London available to a wider audience. Copyright and Moral Rights remain with the author(s) and/or copyright holders. URLs from City Research Online may be freely distributed and linked to.

**Reuse:** Copies of full items can be used for personal research or study, educational, or not-for-profit purposes without prior permission or charge. Provided that the authors, title and full bibliographic details are credited, a hyperlink and/or URL is given for the original metadata page and the content is not changed in any way.



# Numerical Evaluation of the Reliability of Using Single-Story Substructures to Study Progressive Collapse Behaviour of Multi-Story RC Frames

Kai Qian<sup>1\*</sup>, Yun-Hao Weng<sup>1</sup>, Feng Fu<sup>2</sup>, and Xiao-Fang Deng<sup>1</sup>

<sup>1</sup>College of Civil Engineering and Architecture, Guangxi University, 100 Daxue Road, China, 530004.

<sup>2</sup> School of Mathematics, Computer Science and Engineering, City, University of London, U.K.

**Abstract:** Progressive collapse is a global failure for a multi-story building. All stories above the removed column will consequently deform and help redistribute the loads initially withstood by the removed column. However, due to cost and excessive time to be involved, the majority of existing experimental researches regarding progressive collapse rely on single-story beam-column substructures or sub-assemblages. To date, how to use the results from single-story substructures or sub-assemblages to fully or confidently study the behavior of multi-story building is still unclear. Thus, it is imperative to investigate the relationship between the results of single-story substructures and the real behavior of multi-story buildings. Thus, for this purpose, in the present study, a series of planar multi-story reinforced concrete (RC) beam-column substructures were modeled using high-fidelity finite element software LS-DYNA. Firstly, the numerical models were validated by the test results of two three-story planar substructures with different design spans. Secondly, the validated models were explored on various load resistance of each story in the investigated multi-story frame. In addition, the effects of boundary conditions, missing column locations, story numbers on the variation of load resistance were studied in detail using the models.

**Keywords:** Progressive collapse; Multi-Story RC frames; Load transfer mechanism; Numerical simulations; Column removal scenario

\* Corresponding author. E-mail address: [qiankai@gxu.edu.cn](mailto:qiankai@gxu.edu.cn)

## 1. Introduction

Progressive collapse is defined in ASCE/SEI 7 [1] as “the spread of an initial local failure from element to element, eventually resulting in the collapse of an entire structure or a disproportionately large part of it”. To date, there are two main methods to design buildings to mitigate progressive collapse: direct and indirect design methods. For the indirect design method, integrity, redundancy, ductility, and minimum tie-force are required. However, when local damages are triggered, it is difficult to quantitatively evaluate the capacity and behavior of remaining building in resisting progressive collapse based on this method. For the direct design method, alternative load path method is most commonly used as it is event-independent. To understand the behavior of multi-story buildings subjected to sudden column missing scenario, Sasani et al. [2] carried out an on-site test for an actual 10-story reinforced concrete building following the explosive damage of an exterior column. Similarly, a six-story RC infilled-frame building was evaluated following the removal of two adjacent exterior columns simultaneously by Sasani [3]. Song et al. [4] tested a steel frame building subjected to physically removal of four ground columns from one of the perimeter frames to study the load redistribution of the building after each column removal. However, as the service load (live load and partial dead load) was removed prior to on-situ tests, the measured displacement response was little. Majority of on-situ tests only experienced elastic response. The plastic behavior especially for compressive arch action (CAA) and tensile catenary action (TCA) could not be captured and therefore be evaluated in detail. Thus, the majority of existing tests in laboratory regarding progressive collapse were single-story beam-column substructures based on alternative load path method (relied on push-down loading regime). A number of tests [5-13] quantified the effects of geometric characteristic and reinforcing details on the mobilization of CAA and TCA for progressive collapse prevention. It was found that the span/depth ratio has great effects on the mobilization of CAA when the RC frame

1 subjected to the loss of a middle column scenario. In addition, the CAA capacity is sensitive to the  
2 horizontal stiffness provided by the beam ends. However, the amount of longitudinal reinforcements in  
3 the structural concrete members has little effect on developing CAA. The researchers [8] indicated that  
4 the continuous top longitudinal reinforcements contributed to TCA capacity while Yi et al. [14]  
5 indicated that both top and bottom longitudinal reinforcements provided contributed to TCA capacity.

6 Moreover, several studies [15-17] were carried out to evaluate the dynamic response and dynamic  
7 load increase factor of RC beam-column sub-assemblages subjected to sudden column removal  
8 scenario. Qian and Li [15] indicated that the acceleration of the frame after sudden column removal  
9 could be as large as 3.5g, where g is the acceleration of gravity, and the dynamic load increase factor  
10 could be less than 1.38. Qian and Li [16] quantified the slab effects on the dynamic response of RC  
11 frames subjected to the sudden removal of a ground corner column. In addition, they proposed an  
12 equivalent single-degree-of-freedom (SDOF) model to predict the dynamic ultimate load capacity of  
13 the tested specimens. The dynamic load increase factor of tested specimens was ranged from 1.30 to  
14 1.34. Liu et al. [17] investigated the dynamic behavior of steel frames with different connections  
15 subjected to sudden removal of a center column experimentally. The test results indicated that the  
16 dynamic phenomenon may detriment the behavior of steel connections and degrade the progressive  
17 collapse resistance of the substructures.

18 However, the reliability of using single-story substructures to study the behavior of multi-story  
19 buildings is based on the assumption that the stories above the removed column have identical  
20 performance, which is questionable and has not been proved. Weng et al. [18] used high fidelity finite  
21 element (FE) models to investigate the load resisting mechanisms of each story for a multi-story flat  
22 slab structure under a middle column loss scenario. The numerical results indicated that the load  
23 resistance from each story in a multi-story flat slab building was different and the largest load resisting

capacity occurred in the first story. However, for a multi-story RC frame, it may be different to flat slab structures as beams could help to redistribute the loads. In Qian and Li [19], two multi-story frames were tested based on displacement-controlled push-down method. As it is not feasible to test a multi-story frame to assess the load resisting contribution of each story, FE models, which are validated against the experimental tests, are used for deeper understanding of the various load transfer mechanism and load resisting contribution of each floor consequently. Moreover, the effects of the number of stories, boundary conditions, and missing column locations are also studied using the validated numerical models.

## 2. Previous Experimental Work

A quasi-static experimental study on progressive collapse resistance of planar RC beam-column substructures subjected to push-down loading regimes was conducted by Qian and Li [19] and the test results of two bare frames are used to validate the reliability of FE models in this numerical study. These two specimens (BFS and BFL) were one-quarter scaled. They were assumed to be subjected to the loss of a penultimate column. The dimension and reinforcement details of Specimen BFS are shown in Fig. 1. As can be seen in the figure, the beam span was 1800 mm. The story height was 900 mm in the first story and 825 mm in upper stories. The cross section of the beam and column was 90 mm×140 mm and 150 mm×150 mm, respectively. The concrete clear cover was 7 mm and 10 mm for beam and column, respectively. Enlarged foundation base with a size of 400 mm×300 mm was designed at the toe of side columns for fixing. The hoop stirrups with 90 degrees bends were utilized for transverse reinforcements. As it was non-seismically designed, no transverse reinforcements were placed in the joint region. The curtailment of longitudinal reinforcements in the beam was in accordance with Singapore Code CP-65 [20]. The middle column in ground level is assumed removed before test and thus, the middle column was only fabricated the upper two stories. For Specimen BFL,

1 similar reinforcement details and dimensions to Specimen BFS were used except longer span of 2400  
2 mm designed. Average cylinder compressive strength measured on the days of testing for both  
3 specimens was 32.1 MPa. The yield strength of R3, R6, and T10 were 417 MPa, 449 MPa, and 515  
4 MPa, respectively. The ultimate strength of R3, R6, and T10 were 479 MPa, 537 MPa, and 594 MPa.  
5 The measured elongation ratio of R3, R6, and T10 were 9.7 %, 13.3 %, and 16.9 %, respectively. “R”  
6 represents plain reinforcement while “T” represents deformed reinforcement.

7           The typical experimental setup and locations of instrumentations are shown in Fig. 2. As  
8 shown in the figure, the specimens were fixed to the strong floor by the foundation bases, which were  
9 cast monolithically with the side columns. A steel column and a specially designed steel assembly  
10 were installed to avoid unforeseen out-of-plane movement of the specimen. This specially designed  
11 steel assembly only allows vertical movement of the middle column through constraining its rotational  
12 and horizontal movements. A hydraulic jack with a 600 mm stroke was installed on the steel column to  
13 apply vertical load. It should be noted that the displacement-controlled push-down loading method was  
14 adopted in the reference tests [19]. A load cell was installed above the hydraulic jack to measure the  
15 applied vertical load. A roller together with a tension/compression load cell was installed horizontally  
16 at each extension part of the specimen to simulate the horizontal constraints of the beams in the  
17 surrounding bay.

### 18 **3. Numerical Model Development and Validation**

19           To illustrate the variation of load resisting capacity and mechanisms of the beams in different  
20 stores overtly, explicit solver software LS-DYNA [21] was used to build the FE models due to its  
21 numerical stability and various constitutive models available. The FE models were validated based on  
22 the experimental results first. As shown in Fig. 3, similar boundary conditions as experimental tests  
23 were used at the FE models. As gaps were deliberately left near the horizontal constraints for the

1 **facility** of installation, springs were installed horizontally at the beam ends of the extension part. The  
2 stiffness of the spring was determined by the measured horizontal reaction force and horizontal  
3 movements at the ends, which was roughly equal to 80 kN/mm at each beam end with a total of 240  
4 kN/mm.

### 5 **3.1 Element types**

6 Fig. 3 shows the numerical model of Specimen BFS. Concrete is simulated by 8-node solid  
7 elements with reduced integration scheme. This solid formulation only has one integration point in  
8 each element, which can enhance computational efficiency with **the promise** of sufficient accuracy, but  
9 hourglass control should be defined properly when this type of **element** was adopted. Moreover,  
10 reinforcing bars were modeled using 2-node Hughes-Liu beam elements with 2×2 Gauss quadrature  
11 integration at the cross-section. This beam formulation can simulate the behavior of axial force, bi-  
12 axial bending, and finite transverse shear strains [22]. Furthermore, the rigid plates for supports or  
13 loading points were also modeled by 8-node solid elements and the springs for horizontal restraints  
14 were simulated by discrete elements.

### 15 **3.2 Bond-slip relationship simulation**

16 To improve the accuracy of **modeling**, considering **the** bond-slip relationship between  
17 reinforcement and concrete is important, as the perfect bonding assumption used in other models will  
18 cause over-prediction of **load-carrying** capacity and lead to premature fracture of reinforcement due to  
19 stress concentration [23]. In this numerical study, the bond-slip relationship between reinforcement  
20 and concrete material was considered by using keyword \*CONTACT\_1D to define one-dimensional

contact interface between the concrete and rebar elements. Virtual springs are defined between the slave nodes from beam elements and the master nodes from solid elements, and the spring force depends on relative displacements between the slave and master nodes [21]. However, simulating bond-slip behavior for all reinforcements would be complicated and required more computational resources. Based on test results, it was noted that the slip occurred mainly at the beam-column joints and the curtail point of top beam longitudinal reinforcements. As a result, similar to previous studies [24, 25], the CONTACT\_1D function was only used for the beam longitudinal reinforcements at the location of beam-column joints and the reinforcements near curtail points, as shown in Fig. 3. Besides, the remaining reinforcements were assumed to be perfect bonding to concrete using keyword \*Constrained\_Lagrange\_In\_Solid. To calibrate the properties of Contact\_1D, the bond-slip relationship proposed by fib Model Code 2010 [26] was applied. For monotonic loading, the bond stress  $\tau_b$  between concrete and hot-rolled plain bar for pull-out failure can be calculated as following [26]:

$$\begin{cases} \tau_b = \tau_{b\max} (s / s_1)^{0.5} & \text{for } 0 \leq s \leq s_1 \\ \tau_b = \tau_{b\max} = 0.3\sqrt{f_c} & \text{for } s > s_1 \end{cases} \quad (1)$$

Where  $s_1 = 0.1$  mm;  $f_c$  is standard cylinder compressive strength. In the tests, the compressive strength of concrete is 32.1 Mpa. Therefore,  $\tau_{b\max} = 1.70 \text{ MPa}$ .

For the CONTACT\_1D (LS-DYNA) function [21], the bonding relationship between the beam elements and solid elements is assumed to be elastic-perfectly-plastic. After elastic stage, the bond stress would decay following an exponential damage curve. The constitutive law of shear stress  $\tau$  and slip  $s$  is given as [21]:

$$\begin{cases} \tau = G_s s & \text{for } s \leq s_{\max} \\ \tau = \tau_{\max} e^{-h_{\text{dmg}} D} & \text{for } s > s_{\max} \end{cases} \quad (2)$$

where  $G_s$  is bond shear modulus;  $s_{\max}$  is maximum elastic slip;  $h_{\text{dmg}}$  is damage curve exponential coefficient;  $D$  is damage parameter, which is equals  $(s-s_{\max})$ .

The comparison between Eqs. (1) and (2) indicates that the values of  $h_{\text{dmg}}$  and  $\tau_{\max}$  are equal to 0 and 1.7 Mpa, respectively. Based on the suggestion from Pham et al. [24] and Yu et al. [25],  $s_{\max} = 0.5 s_I = 0.05$  mm. Therefore,  $G_s = \tau_{\max} / s_{\max} = 34 \text{ MPa} / \text{mm}$ . The comparison of the bond-slip relationship between the fib Model Code 2010 [26] and the suitable model used in CONTACT\_1D is shown in Fig. 4.

### 3.3 Material model

In this study, Continuous surface cap model (CSCM) is chosen to simulate concrete material. This model can effectively model damage-based softening and modulus reduction, shear dilation, shear compaction, confinement effect, and strain rate effect under low constraint conditions [27]. Previous studies had proven its accuracy in the simulation of RC components under both quasi-static and dynamic conditions [24, 25, 28].

The CSCM provides a simplified version (\*Mat\_CSCM\_CONCRETE) for concrete materials with the compressive strength between 28 Mpa and 48 Mpa. The default parameters depend on three input parameters: unconfined compressive strength  $f'_c$ , maximum aggregate size  $A_g$ , and units. For both Specimens BFS and BFL,  $f'_c$  and  $A_g$  are 32.1 Mpa and 8 mm, respectively. The CSCM also provides a strain-based approach of erosion algorithm to simulate material failure, and the related parameter is “ERODE”. When the “ERODE” is set greater than 1.0, the concrete elements would be deleted if damage index exceeds 0.99 and the maximum principal strain exceeds (ERODE-1.0) according to LS-DYNA keyword user’s manual [21]. This feature is used here to effectively model the failure mode of the frame. In the reference test results, the failure modes of the multi-story frames were governed by

1 the flexure and tensile actions, primarily denoted by the formation of severe cracks at the beam ends  
2 near the center column and at the curtail points of beam top longitudinal reinforcements. Therefore, the  
3 maximum principal strain is a suitable criterion for erosion algorithm. The value of “ERODE” is mesh-  
4 dependent, and set as 1.10, corresponding to the maximum principal of 0.1, for element size 20 mm  
5 according to the previous work [24]. The strain rate effect of the CSCM is ignored because only quasi-  
6 static behavior is considered.

7 The isotropic elastic-plastic material model Mat\_Plastic\_Kinematic (MAT\_003) is used to model  
8 reinforcements. The elastic modulus, yield strength, tangential modulus after yielding, and ultimate  
9 strain is determined based on properties of steel bars. Also, the strain rate effect is excluded.

10 As choosing the appropriate mesh size is important to obtain reliable and effective results, mesh  
11 sensitivity is evaluated. Four different mesh sizes of elements (side length for solid elements and  
12 length for beam elements), including 30 mm, 25 mm, 20 mm, and 15 mm, were employed for  
13 Specimen BFS. The results of the load-removed column displacement (RCD) relationship for different  
14 mesh sizes are shown in Fig. 5. Obviously, mesh size of 20 mm is adequate, as further mesh  
15 refinement is not able to cause any remarkable convergence but instead taking larger computational  
16 resources. As a result, the mesh size is chosen as 20 mm.

17 However, based on the default parameters of the CSCM, the numerical models will overestimate  
18 the initial stiffness and load resisting capacity of the specimens, as shown in Fig. 6. Unconfined  
19 uniaxial stress-strain relationship for 32.1 MPa based on the default parameters of the CSCM is shown  
20 in Fig. 7. As can be seen from the figure, the compressive strength is attained at a strain of 0.001. But  
21 in reality, when normal strength concrete reaches its compressive strength, the strain is usually at about  
22 0.002. Therefore, the elastic modulus of concrete should be reduced properly to improve the numerical  
23 results, which had been pointed out by Yu et al. [25]. On the other hand, Yu et al. [25, 28] suggested

that the tensile fracture energy  $G_{ft}$  could be reduced to 80 % of the default one when the simulating result is over predicted. If shear or compressive based damage is significant, then setting  $G_{fs}$  (compressive fracture energy) = 0.5  $G_{ft}$  and  $G_{fc}$  (shear fracture energy) = 50  $G_{ft}$  is reasonable [25]. However, the default ones are assumed as  $G_{fs}=G_{ft}$  and  $G_{fc}=100G_{ft}$ . Since severe shear cracks were formed in the exterior joint in the first floor and the concrete crushing was not obvious during testing, only the reduced shear fracture energy is used for the CSCM model herein. The user-specified material property inputs for CSCM are listed in Table 1. When the adjusted material property is used for simulating, the stiffness of the unconfined uniaxial compression is lower than that of the default one and the compressive stress reduces faster in the softening stage, as shown in Fig. 7. However, the adjusted material property can improve the numerical results significantly, as shown in Fig. 6. Therefore, these adjustments are finally used to simulate Specimens BFS and BFL.

### 3.4 Verification of numerical model

Fig. 8 shows the comparison of load-displacement curves from numerical simulation and experimental results. Generally, the FE models can simulate all three stages of the structural responses well. In the first stage, the structural resistance increases until reaching the first peak load. The resistance is attributed into the flexural action and compressive arch action (CAA). Then, the resistance decreases due to the weakening of CAA in the second stage. In the last stage, the resistance increases again due to the development of tensile catenary action (TCA), and abrupt reduction since rebar fracture was also simulated. For Specimens BFS and BFL, the error between the predicted and measured peak capacity is less than 10 %, as shown in Fig. 8.

Fig. 9 shows the comparison of the simulated and measured horizontal displacement responses at exterior joints. In general, the FE models could predict the horizontal movements of the joints well

including the inward and outward movements and transition phase. In CSCM, the contour plot of effective plastic strain could indirectly reflect the crack pattern of the specimens as the crack pattern could not be physically displayed in LS-DYNA [24]. Figs. 10 and 11 compare the failure modes of test specimens from numerical simulations and experimental results. In **general**, the FE models could simulate the failure modes and crack patterns well including the positions of rebar fracture and concrete spalling. Therefore, the validated FE models were utilized to further study the effects of boundary conditions, locations of column missing, and story numbers on the varying load transfer mechanism in floors.

#### **4. Detailed Discussion of the Numerical Results**

##### ***4.1 Load transfer mechanisms of planar multi-story RC frames***

As mentioned above, most of **the** existing tests on progressive collapse research are single-story beam-column substructures or sub-assemblages due to cost and time consideration. However, progressive collapse is a global behavior for a multi-story building, and the load transfer mechanisms may not be the same in **each** story, especially for the asymmetric structure. Therefore, it is necessary to investigate the various load transfer mechanisms of each floor of the frame model. However, the horizontal constraints of the test specimens were simplified due to the limitation of the cast and testing space. Therefore, to get a more realistic response of structures, a five-span planar frame model with penultimate column loss named BFS-P was built based on the verified **modeling** techniques in BFS, as shown in Fig. 12. Comparing to BFS, BFS-P has a close-to-reality boundary condition provided by the beams in surrounding bay. Therefore, BFS-P could be the key reference model in this numerical simulation program. To understand the effect of story numbers on the load transfer mechanism of planar RC beam-column substructures subjected to progressive collapse, BFS-P-5F with five stories,

1 BFS-P-7F with seven stories, and BFS-P-9F with nine stories were also modeled based on the model  
2 BFS-P, as shown in Fig. 13.

#### 3 *4.2 Structural resistance of each story*

4 The structural resistance of each story equals the summation of vertical loads on both sides of the  
5 beam section located above the removed column. Fig. 14 illustrates the load resistance of each story in  
6 specimen BFS-P. As shown in the figure, the load resistance of each story is different after elastic  
7 stage. It can be seen that the first story contributed the greatest load resistance when the RCD is less  
8 than 133 mm or larger than 220 mm. In terms of CAA capacity, the resistance from the third story is  
9 larger than that of the second story and the biggest one is measured in the first story. Regarding the  
10 TCA stage, the biggest TCA capacity is also measured in the first story. In general, the assumption of  
11 each story demonstrating the same load transfer mechanisms and resistance, which is the basic  
12 assumption to use the behavior of a single-story substructure to represent a real multi-story frame, is  
13 not accurate for planar frames subjected to a penultimate column missing scenario.

14 Figs. 15, 16, and 17 show the story resistance results of BFS-P-5F, BFS-P-7F, and BFS-P-9F,  
15 respectively. Similar to BFS-P, the story resistance began diverging after the elastic stage, and the  
16 resistance of the first story is larger than the ones of other stories when the RCD is less than 133 mm  
17 or greater than 216 mm. Besides, prior to the fracture of longitudinal reinforcements, the load  
18 resistance of the middle stories is quite similar, indicating that the middle stories have similar load  
19 transfer mechanisms. To reveal the behavior of multi-story frame subjected to the loss of a column  
20 scenario, commonly utilized single-story sub-assembly tests may be insufficient. To the contrary,  
21 three sub-assembly tests (top story, one of middle story, and ground story) with proper boundary  
22 conditions were required.

### 1    *4.3 Development of axial forces in beams*

2            To reveal the difference of load transfer mechanism of the beams in each story, the results of the  
3    beam axial force of BFS-P were also extracted and presented in Fig. 18. As the axial force throughout  
4    each beam is identical, the development of the axial force of the whole beam can be represented by  
5    that of one arbitrary section at the beam. Due to asymmetry, the axial force of the beams at different  
6    sides of the removed column may be different. Therefore, the axial forces of the beam sections, which  
7    are at a distance of 200 mm away from the beam-column interface, were extracted. The labels of L1 to  
8    L3 represent the sections at the left side of the removed column (called interior bay) while the labels of  
9    R1 to R3 represent the sections at the right side of the removed column (called exterior bay).

10           In elastic stage, the beams in the first and second stories are in tension while the beam in third  
11    story is in compression. These beams worked like a large composite beam under flexure. After elastic  
12    stage, as shown in Fig. 18a, the interior-bay beam in the first story (IB-beam-1<sup>st</sup>) begins to develop  
13    compressive force initially and achieved the maximum compressive force of -17.0 kN at a RCD of 108  
14    mm. After that, the axial force of the IB-beam-1<sup>st</sup> starts to decrease, and changes into tension at a RCD  
15    of 208 mm. Different from the IB-beam-1<sup>st</sup>, the axial force of the interior-bay beam in the second story  
16    (IB-beam-2<sup>nd</sup>) is in tension initially, and it transfers to compression at a RCD of 74 mm. The  
17    maximum compressive force of the IB-beam-2<sup>nd</sup> is -4.0 kN, which is only 23.5 % of the one of the IB-  
18    beam-1<sup>st</sup>. Moreover, the axial force of the IB-beam-2<sup>nd</sup> transfers to tension again at a RCD of 308 mm.  
19    For the interior-bay beam in the third story (IB-beam-3<sup>rd</sup>), the beam is in compression until the RCD  
20    reaches 266 mm, and the maximum compressive force is -10.0 kN, which is 58.8 % of the one of the  
21    IB-beam-1<sup>st</sup>. Besides, the maximum tensile forces of IB-beam-1<sup>st</sup>, IB-beam-2<sup>st</sup>, and IB-beam-3<sup>st</sup> are  
22    27.0 kN, 11.9 kN, and 8.4 kN, respectively. For the exterior bay, as shown in Fig. 18b, the

1 development of the axial force of the exterior-bay beam in the first story (EB-beam-1<sup>st</sup>) is quite similar  
2 to the one of the IB-beam-1<sup>st</sup>, which is in compression first and finally in tension. Due to interaction of  
3 the beam-column elements among stories, the exterior-bay beam in the second story (EB-beam-2<sup>st</sup>) is  
4 in tension first and in compression slight after RCD of 250 mm. However, the exterior-bay beam in  
5 third story (EB-beam-3<sup>rd</sup>) is always in compression during the whole loading history. In a word, the  
6 distributions of axial forces in both interior-bay and exterior-bay beams indicate the CAA could  
7 develop in the first and third stories, whereas flexural action is the main mechanism of second story to  
8 redistribute the gravity load. Moreover, the significant axial tensile forces of the IB-beam-1<sup>st</sup> and EB-  
9 beam-1<sup>st</sup> in the large deformation stage also illustrate the TCA could develop in the first story beams  
10 effectively.

11 Figs. 19, 20, and 21 show the development of the axial forces in the beams of different stories for  
12 BFS-P-5F, BFS-P-7F, and BFS-P-9F, respectively. It is observed that the beam axial forces in the  
13 middle stories is quite similar. Most of the beam axial forces in the middle stories are mainly in tension  
14 first, and the compressive force appears at large deflection stage, indicating that flexural action is the  
15 main mechanism of these stories to balance the gravity load. On the other hand, the beam axial forces  
16 of the top and bottom stories are similar to the ones of BFS-P. Similarly, the greatest compressive and  
17 tensile forces are measured in the first story, which indicates CAA and TCA can develop in the first  
18 story effectively. Further parametric study in Section 5.2 will evaluate the accuracy of the conclusion  
19 for the frames subjected to interior or corner removal scenarios.

## 1    **5. Parametric Study on Planar Multi-Story RC Frame**

### 2    ***5.1 Effect of boundary conditions***

3        As shown in Fig. 2, in the referenced tests [19], the horizontal constraints of the beams in  
4    surrounding bay were simplified due to the limitation of the cast and testing space. However, the  
5    reliability of the simplification has not been evaluated properly. To quantify the effect of the horizontal  
6    restraint stiffness provided by the surrounding bay, four different horizontal restraint stiffness,  
7    including 0, 15 kN/mm, 150 kN/mm and rigid, were used for the models of BFS and BFL.

8        Fig. 22 shows the load-displacement curves of BFS and BFL with different boundary conditions.  
9    It should be noted that the results of tests are similar to that with rigid restraints for both Specimens  
10   BFS and BFL. As shown in Fig. 22, when the horizontal restraint stiffness decreases from rigid to 0,  
11   the first peak load (FPL) of BFS and BFL decreases to 87 % and 90 %, respectively, due to weakened  
12   CAA. However, reducing the horizontal restraint stiffness is not sensitive to the structural resistance at  
13   large deflection stage. Even though there are no spring restraints applied, both BFS and BFL can  
14   develop TCA in the initial stage. This is because the remaining two side columns can provide  
15   sufficient lateral stiffness to develop TCA initially. However, the TCA weakens due to damage of the  
16   side columns later.

17        As shown in Fig. 22a, the FPL of BFS-P, which has a more real boundary condition, is 92 % of  
18   that of the BFS. It means that the horizontal restraint stiffness used in the tests may be larger than the  
19   real one.

## 1    **5.2 Effect of location of removed column**

2        For the referenced tests [19], only the scenario of missing a penultimate column is investigated.  
3        Two extra numerical models, which were called BFS-I (an interior column was removed in advance)  
4        and BFS-C (a corner column was removed in advance), were built to investigate the effects of different  
5        column removal scenarios on the load transfer mechanism of each story, as shown in Fig. 23. Fig. 24  
6        shows the decomposition of the load resistance of BFS-I. Similar to BFS-P, the first story achieves the  
7        highest initial stiffness and provides the majority of CAA and TCA capacity. However, different from  
8        BFS-P, the resistances of the second and third stories are almost the same before RCD reached 285  
9        mm. The difference in the load resistance of these two stories is mainly due to the mobilization of  
10       TCA in the second story. As shown in Fig. 25, when RCD exceeds 285 mm, the beams of the second  
11       story start to be in tension, indicating the TCA starts to develop in second story too.

12       For BFS-C, as shown in Fig. 26, the FPL of the first story is also the largest among stories.  
13       However, the second story achieves the second largest one, which is different to BFS-P and BFS-I.  
14       The different resistance mechanism is due to interaction of the beam-column elements among stories  
15       (Vierendeel action).

## 16    **6. Conclusions**

17       Based on the numerical and parametric studies conducted in this study, the following conclusions  
18       are drawn:

19       1. Comparing with experimental results, it is found that high fidelity numerical models are able  
20       to accurately simulate the global behavior of the planar multi-story RC frame subjected to a  
21       penultimate column loss scenario.

22       2. For a planar multi-story RC frame subjected to a penultimate column removal scenario, the

1 load transfer mechanism of **each** story is not identical. However, when increasing the number of stories,  
2 it can be found that the load transfer mechanism of the middle stories is almost the same. Therefore,  
3 the behavior of a planar multi-story frame should be equivalently investigated by three types of single-  
4 story beam-column assemblies (top-story, middle-story, and ground-story) with proper boundary  
5 conditions.

6 3. Horizontal restraint stiffness can significantly affect the development of CAA. Reducing the  
7 restraint stiffness of the horizontal springs would decrease the FPL of the frames due to the weakening  
8 of CAA. When the horizontal restraint stiffness decreases from rigid to 0, the FPL of BFS and BFL  
9 decreases by 87 % and 90 %, respectively. However, horizontal restraint stiffness affecting is  
10 insensitive to the development of TCA. Even though spring restraint stiffness reduces to 0, the rest of  
11 side columns can provide enough constraints to develop TCA partially.

12 4. It is found from the comparison of the load-displacement curves between the specimens BFS-  
13 P and BFS that the load capacity of the Specimen BFS-P is relatively less than that of the Specimen  
14 BFS. It means that the horizontal constraints applied on the tests may be stronger than the real one,  
15 which will overestimate the capacity of the structure to mitigate progressive collapse.

16 5. Numerical analysis on different column removal scenarios indicates that the beams from a  
17 planar multi-story RC frame subjected to progressive collapse demonstrate different load resistance.  
18 However, the beam in the first story achieves the greatest initial stiffness and load resisting capacity  
19 regardless of the location of removed column.

20

## 21 **Acknowledgments**

22 The authors gratefully acknowledge the financial support provided by the Natural Science  
23 Foundation of China (Nos. 51778153, 51568004, 51478118). The high-level innovation team in

colleges and universities and excellence scholar program in Guangxi (201738). Any opinions, findings and conclusions expressed in this paper do not necessary reflect the view of Natural Science Foundation of China.

## References

- [1] ASCE/SEI 7. Recommendations for designing collapse-resistant structures. Structural Engineering Institute-American Society of Civil Engineers, 2010, Reston, VA.
- [2] M. Sasani, M. Bazan, S. Sagioglu, Experimental and analytical progressive collapse evaluation of actual reinforced concrete structure, *ACI Structural Journal* 104(6) (2007) 731-739.
- [3] M. Sasani, Response of a reinforced concrete infilled-frame structure to removal of two adjacent columns, *Engineering Structures* 30(9) (2008) 2478-2491.
- [4] B.I. Song, K.A. Giriunas, H. Sezen, Progressive collapse testing and analysis of a steel frame building, *Journal of Constructional Steel Research* 94 (2014) 76-83.
- [5] Y.P. Su, Y. Tian, X.S. Song, Progressive collapse resistance of axially-restrained frame beams, *ACI Structural Journal* 106(5) (2009) 600-607.
- [6] M. Sasani, A. Werner, A. Kazemi, Bar fracture modeling in progressive collapse analysis of reinforced concrete structures, *Engineering Structures* 33(2) (2011) 401–409.
- [7] I. Azim, J. Yang, S. Bhatta, F. Wang, Q-F. Liu, Factors Influencing the progressive collapse resistance of RC frame Structures. *Journal of Building Engineering*, 2020; 27.
- [8] J. Yu, K.H. Tan, Experimental and numerical investigation on progressive collapse resistance of reinforced concrete beam column sub-assemblages, *Engineering Structures* 55 (2013) 90-106.
- [9] N. FarhangVesali, H. Valipour, B. Samali, S. Foster, Development of arching action in longitudinally-restrained reinforced concrete beams. *Construction and Building Materials* 47 (2013) 7–19.

- 1 [10]K. Qian, B. Li, J.X. Ma, Load-carrying mechanism to resist progressive collapse of RC buildings,  
2 Journal of Structural Engineering 141(2) (2015) 04014107.
- 3 [11]K. Qian, B. Li, Z. Zhang, Influence of multicolumn removal on the behavior of RC floors, Journal  
4 of Structural Engineering 142(5) (2016) 04016006.
- 5 [12]P.Q. Ren, Y. Li, X.Z. Lu, H. Guan, Y.L. Zhou, Experimental investigation of progressive collapse  
6 resistance of one-way reinforced concrete beam-slab substructures under a middle-column-removal  
7 scenario, Engineering Structures 118 (2016) 28–40.
- 8 [13]X.Z. Lu, K.Q. Li, C.F. Li, Y. Li, New analytical calculation models for compressive arch action in  
9 reinforced concrete structures, Engineering Structures 168 (2018) 721-735.
- 10 [14]W.J. Yi, Q.F. He, Y. Xiao, S.K. Kunnath, Experimental study on progressive collapse-resistant  
11 behavior of reinforced concrete frame structures, ACI Structural Journal 105(4) (2008) 433-439.
- 12 [15]K. Qian, B. Li, Dynamic performance of RC beam-column substructures under the scenario of the  
13 loss of a corner column-experimental results, Engineering Structures 42 (2012) 154-167.
- 14 [16]K. Qian, B. Li, Quantification of slab influence on the dynamic performance of RC frames against  
15 progressive collapse, Journal of Performance of Constructed Facilities 29(1) (2015) 04014029.
- 16 [17]C. Liu, K.H. Tan, T.C. Fung, Component-based steel beam-column connections modeling for  
17 dynamic progressive collapse analysis, Journal of Constructional Steel Research 107 (2015) 24-36.
- 18 [18]Y.-H. Weng, K. Qian, F. Fu, Q. Fang, Numerical investigation on load redistribution capacity of  
19 flat slab substructures to resist progressive collapse, Journal of Building Engineering 29 (2020)  
20 101109.
- 21 [19]K. Qian, B. Li, Effects of masonry infill wall on the performance of RC frames to resist  
22 progressive collapse, Journal of Structural Engineering 143(9) (2017) 04017118.

- [20] CP 65. Structural use of concrete, part 1. Code of practice for design and construction. Singapore Standard, 1999.
- [21] J. Hallquist, LS-DYNA keyword user's manual, Version 971, Livermore Software Technology Corporation, 2007, Livermore, CA.
- [22] J. Hallquist, LS-DYNA theoretical manual. Livermore Software Technology Corporation, 1998, Livermore, CA.
- [23] Y. Bao, H.S. Lew, S.K. Kunnath, Modeling of reinforced concrete assemblies under column-removal scenario, *Journal of Structural Engineering* 140(1) (2014) 04013026.
- [24] A.T. Pham, K.H. Tan, J. Yu, Numerical investigations on static and dynamic responses of reinforced concrete sub-assemblages under progressive collapse, *Engineering Structures* 149 (2017) 2-20.
- [25] J. Yu, L. Luo, Y. Li, Numerical study of progressive collapse resistance of RC beam-slab substructures under perimeter column removal scenarios, *Engineering Structures* 159 (2018) 14-27.
- [26] Betonbau. Fib model code for concrete structures 2010. Ernst & Sohn 2013.
- [27] Y. Wu, J.E. Crawford, J.M. Magallanes, Performance of LS-DYNA concrete constitutive models, 12th Int. LS-DYNA Users Conf., Livermore Software Technology Corporation, 2012, Livermore, CA.
- [28] J. Yu, Y.P. Gan, J. Wu, H. Wu, Effect of concrete masonry infill walls on progressive collapse performance of reinforced concrete infilled frames, *Engineering Structures* 191 (2019) 179-193.

## Captions of tables

**Table 1-** Model parameters of CSCM after adjustment (Units: N, mm and ms)

## Captions of figures

**Fig. 1**–Reinforcement layout of the Specimen BFS: (a) Elevation view, (b) Cross section of RC frame

Note: Unit in mm, T=Deformed reinforcing bar; R=Plain reinforcing bar

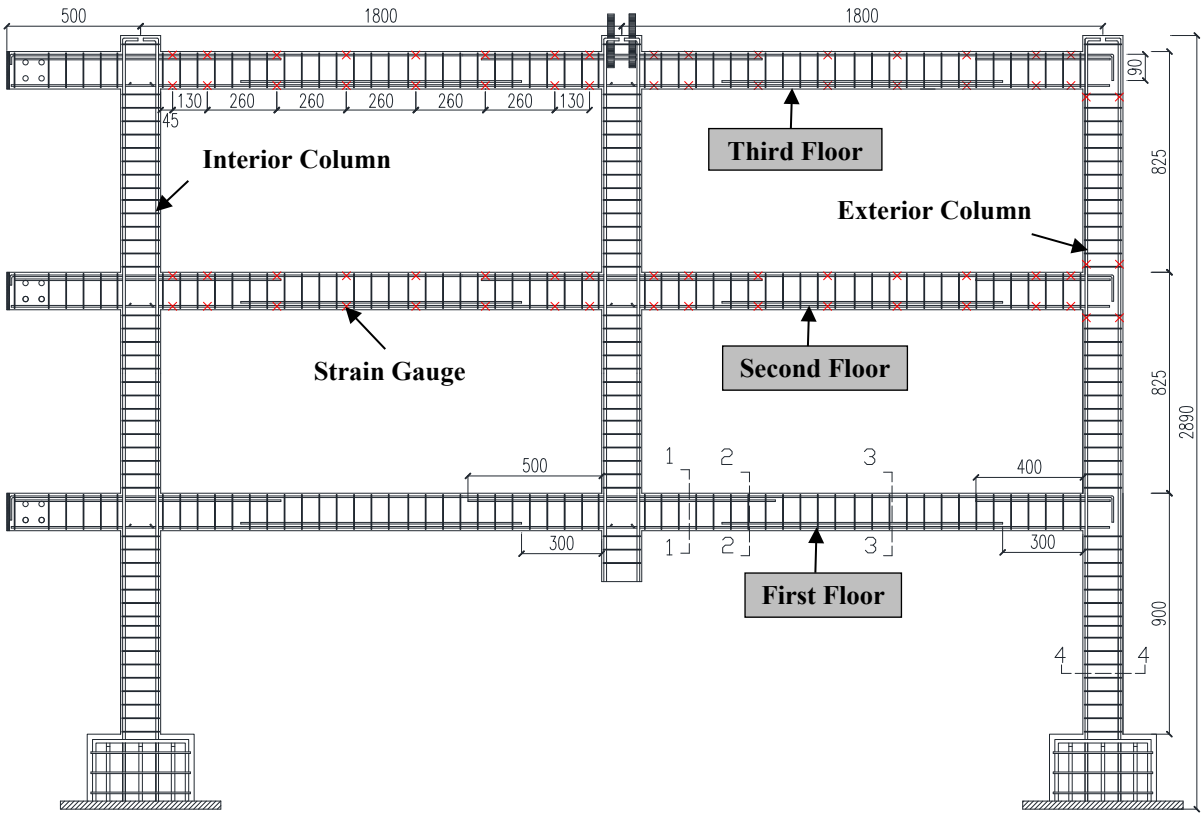
- 1 **Fig. 2**–Test setup and instrumentation
- 2 **Fig. 3**–Numerical model of Specimen BFS
- 3 **Fig. 4**–Comparison of bond-slip relationship between Model Code 2010 and Contact\_1D
- 4 **Fig. 5**–Comparisons of different mesh sizes
- 5 **Fig. 6**–Comparisons of different concrete input parameters
- 6 **Fig. 7**–Unconfined uniaxial stress-strain relationship of concrete for 32.1 MPa based on CSCM
- 7 **Fig. 8**–Comparison of the load-displacement between simulation and test: (a) BFS, (b) BFL
- 8 **Fig. 9**– Comparison of the horizontal movement response from numerical and test: (a) BFS, (b) BFL
- 9 **Fig. 10**–Comparisons of damage patterns of BFS: (a) FEM, (b) Test
- 10 **Fig. 11**–Comparisons of damage patterns of BFL: (a) FEM, (b) Test
- 11 **Fig. 12**–Numerical model of BFS-P
- 12 **Fig. 13**–Numerical models of number of different floors: (a) BFS-P-5F, (b) BFS-P-7F, (c) BFS-P-9F
- 13 **Fig. 14**–Load resistance of each story of BFS-P
- 14 **Fig. 15**–Load resistance of each story of BFS-P-5F
- 15 **Fig. 16**–Load resistance of each story of BFS-P-7F
- 16 **Fig. 17**–Load resistance of each story of BFS-P-9F
- 17 **Fig. 18**–Development of beam axial forces of BFS-P: (a) Left side of removed column, (b) Right side
- 18 of removed column
- 19 **Fig. 19**–Development of beam axial forces of BFS-P-5F: (a) Left side of removed column, (b) Right
- 20 side of removed column
- 21 **Fig. 20**–Development of beam axial forces of BFS-P-7F: (a) Left side of removed column, (b) Right
- 22 side of removed column
- 23 **Fig. 21**–Development of beam axial forces of BFS-P-9F: (a) Left side of removed column, (b) Right
- 24 side of removed column
- 25 **Fig. 22**–Comparison of different boundary conditions: (a) BFS, (b) BFL,
- 26 **Fig. 23**–Numerical models of different column loss: (a) BFS-I, (b) BFS-C
- 27 **Fig. 24**–Load resistance of each story of BFS-I
- 28 **Fig. 25**–Development of beam axial forces of BFS-I
- 29 **Fig. 26**–Load resistance of each story of BFS-C
- 30
- 31
- 32

1  
2  
3  
4  
5  
6

**Table 1**  
Model Parameters of CSCM after Adjustment (Units: N, mm and ms)

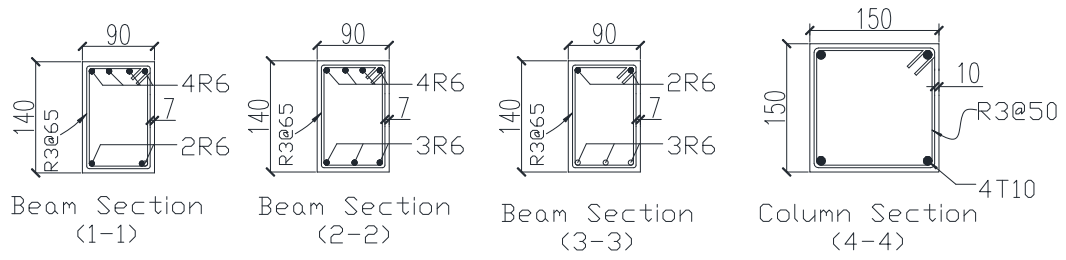
|         |          |        |         |           |          |        |         |
|---------|----------|--------|---------|-----------|----------|--------|---------|
| MID     | RO       | NPLOT  | INCRE   | IRATE     | ERODE    | RECOV  | ITRETRC |
| 1       | 0.00232  | 1      | 0.0     | 0         | 1.10     | 0.0    | 0       |
| PRED    |          |        |         |           |          |        |         |
| 0       |          |        |         |           |          |        |         |
| G       | K        | ALPHA  | THETA   | LAMDA     | BETA     | NH     | CH      |
| 7065    | 7738     | 14.788 | 0.3029  | 10.5      | 0.01929  | 0      | 0       |
| ALPHA1  | THETA1   | LAMDA1 | BETA1   | ALPHA2    | THETA2   | LAMDA2 | BETA2   |
| 0.74735 | 0.001102 | 0.17   | 0.06855 | 0.66      | 0.001323 | 0.16   | 0.06855 |
| R       | XD       | W      | D1      | D2        |          |        |         |
| 5.0     | 91.5     | 0.05   | 2.5e-04 | 3.492e-07 |          |        |         |
| B       | GFC      | D      | GFT     | GFS       | PWRC     | PWRT   | PMOD    |
| 100.0   | 4.575    | 0.1    | 0.04575 | 0.02288   | 5.0      | 1.0    | 0.0     |
| ETA0C   | NC       | ETAOT  | NT      | OVERC     | OVERT    | SRATE  | REPOW   |
| 0       | 0        | 0      | 0       | 0         | 0        | 0      | 0       |

7  
8  
9



(a)

10  
11



(b)

**Fig. 1**—Reinforcement layout of the Specimen BFS: (a) Elevation view, (b) Cross section of RC frame

Note: Unit in mm, T=Deformed reinforcing bar; R=Plain reinforcing bar

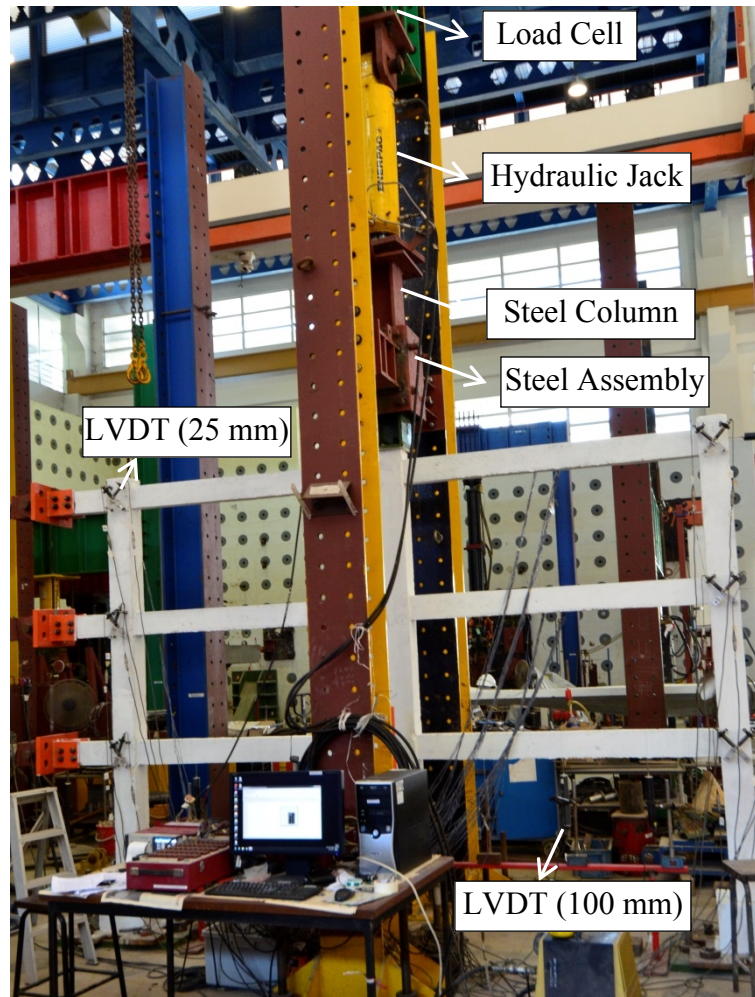


**Fig. 2**—Test setup and instrumentation

1

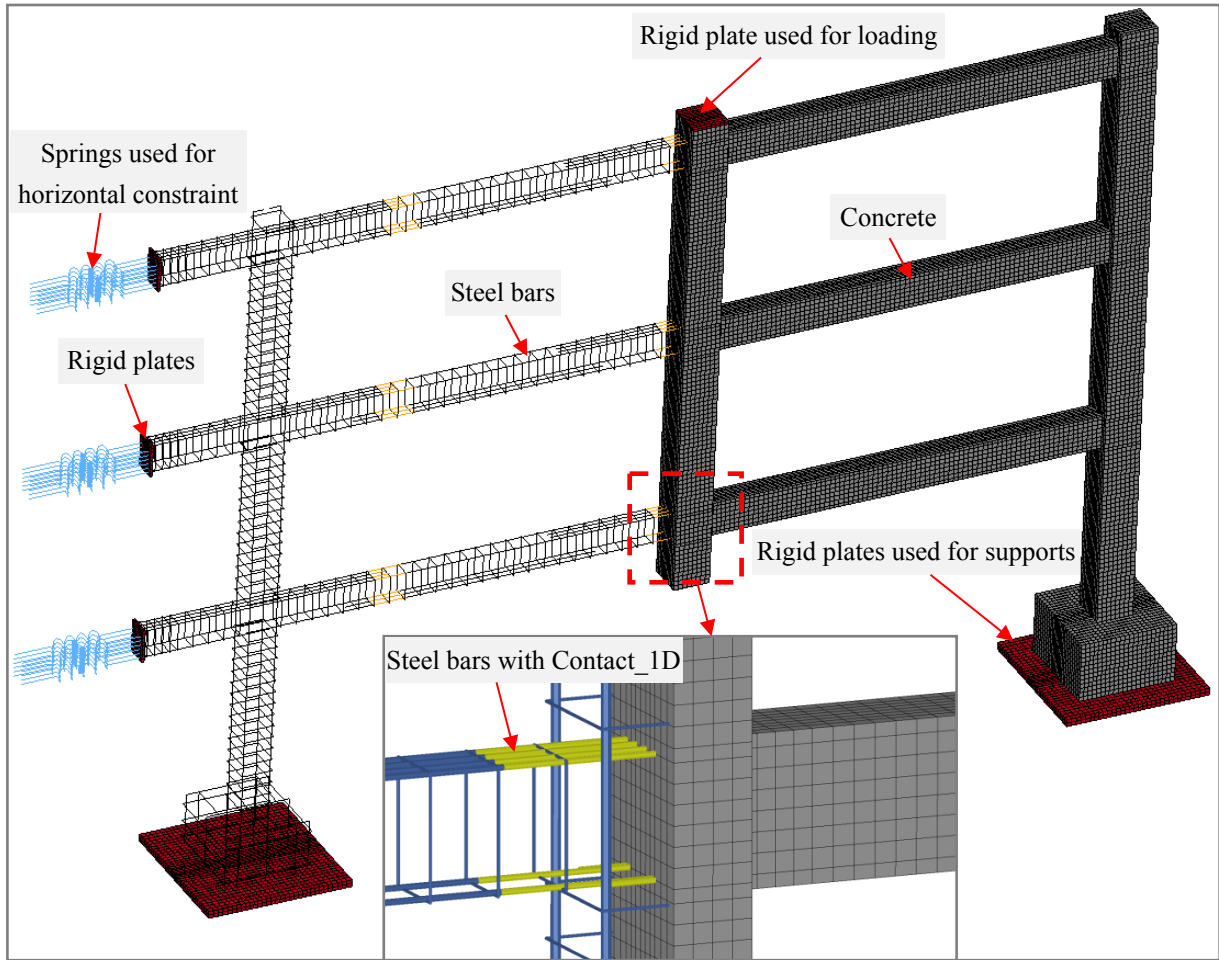


**Fig. 3**—Geometric model of Specimen BFS

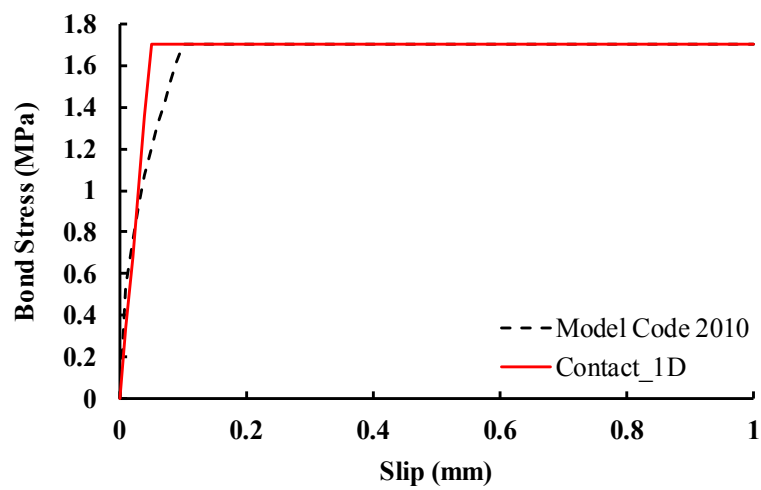


**Fig. 4**—Comparison of bond-slip relationship between Model Code 2010 and Contact\_1D

1

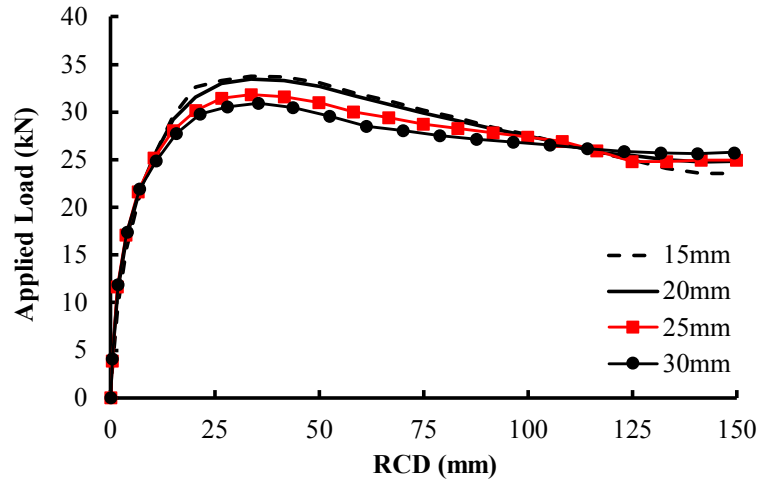


**Fig. 5**–Effects of different mesh sizes

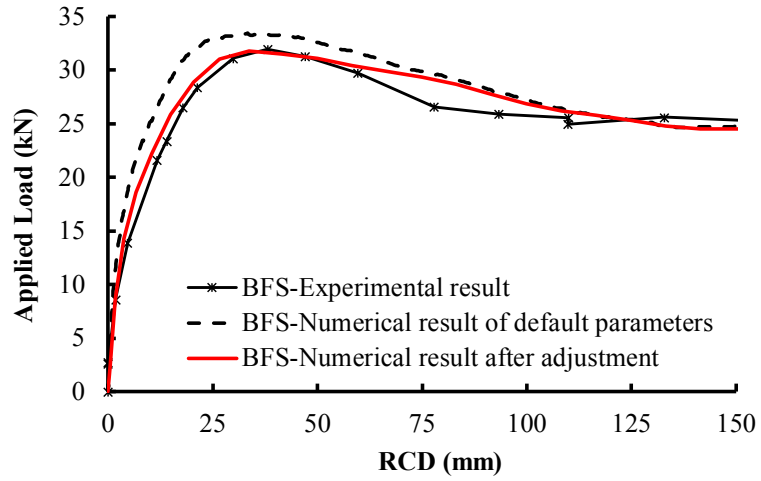


**Fig. 6**–Effects of different concrete input parameters

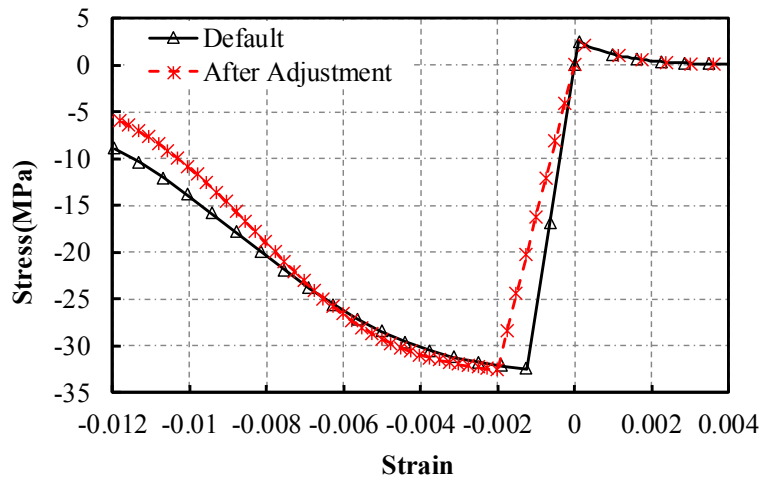
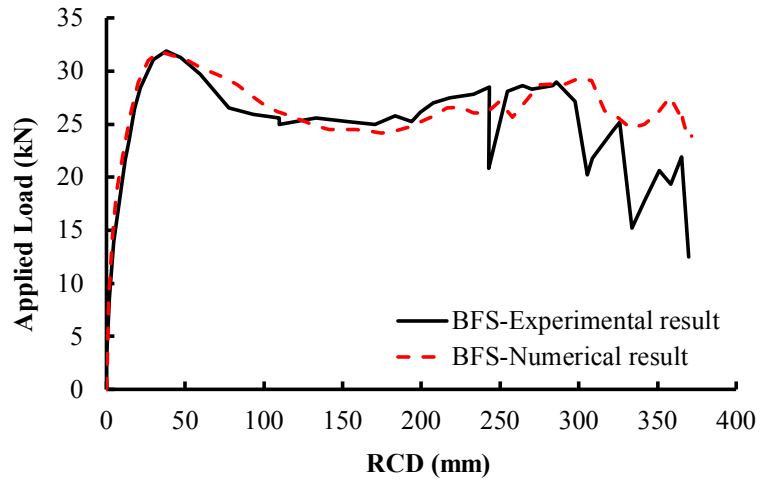
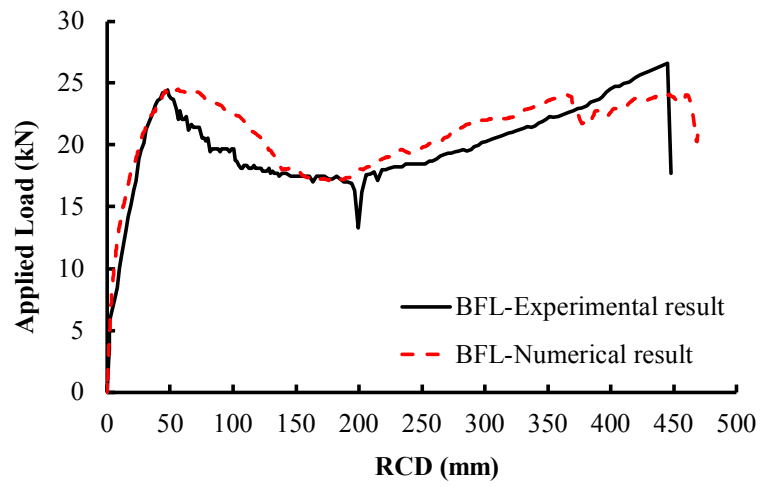


**Fig. 7**–Unconfined uniaxial stress-strain relationship of concrete for 32.1 MPa based on CSCM

1

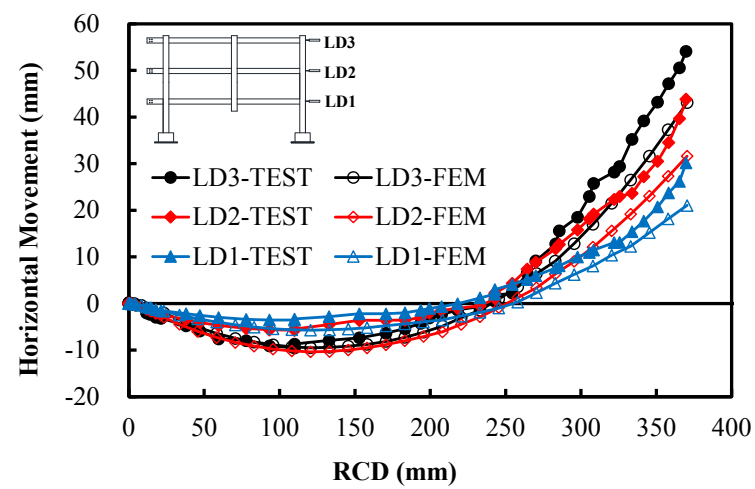


(a)

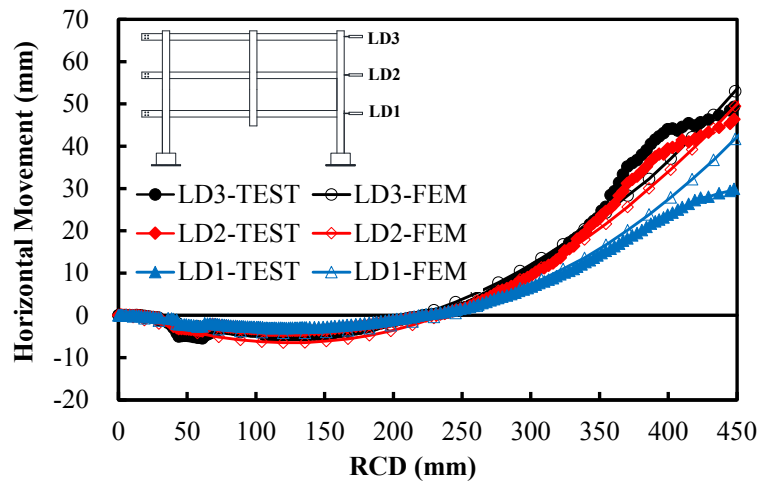


(b)

**Fig. 8**—Comparison of the load-displacement response from numerical and test: (a) BFS, (b) BFL

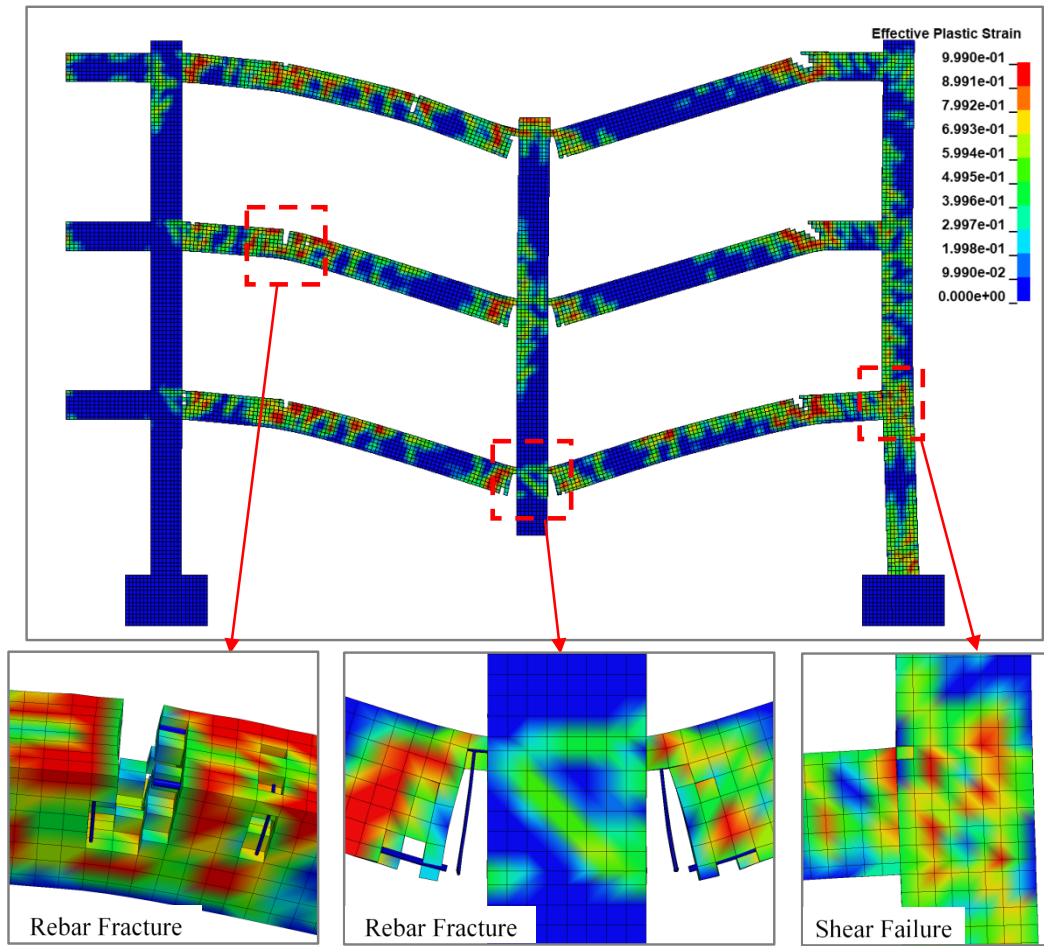


(a)

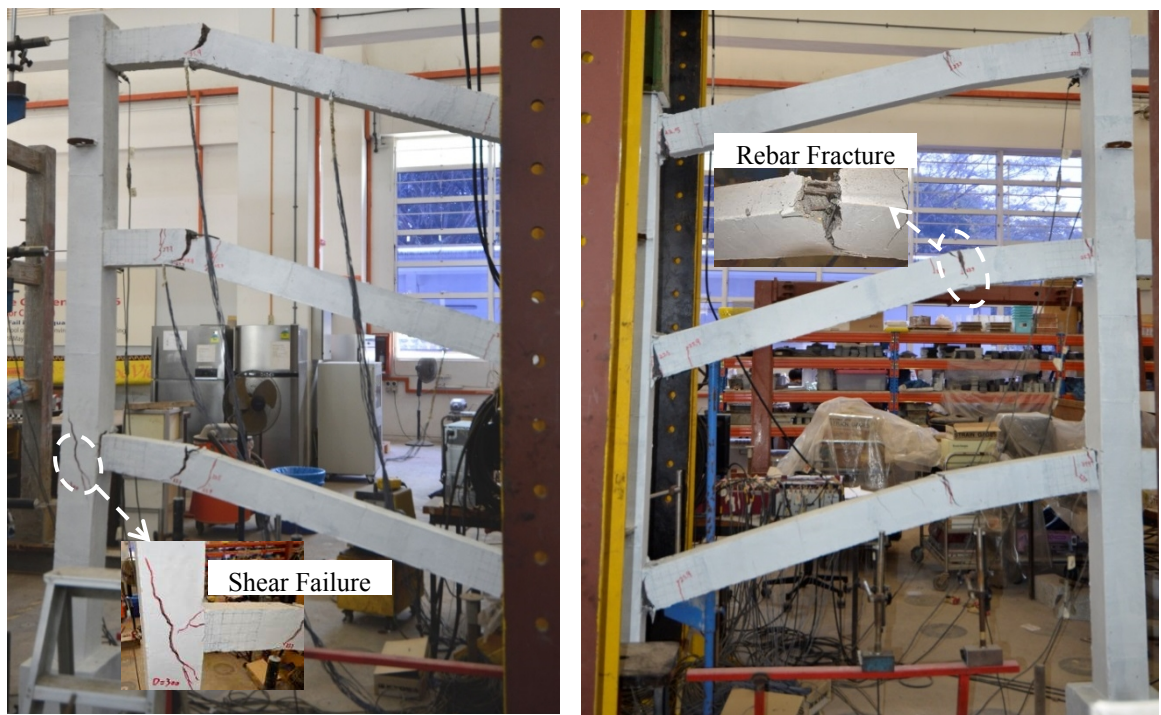


(b)

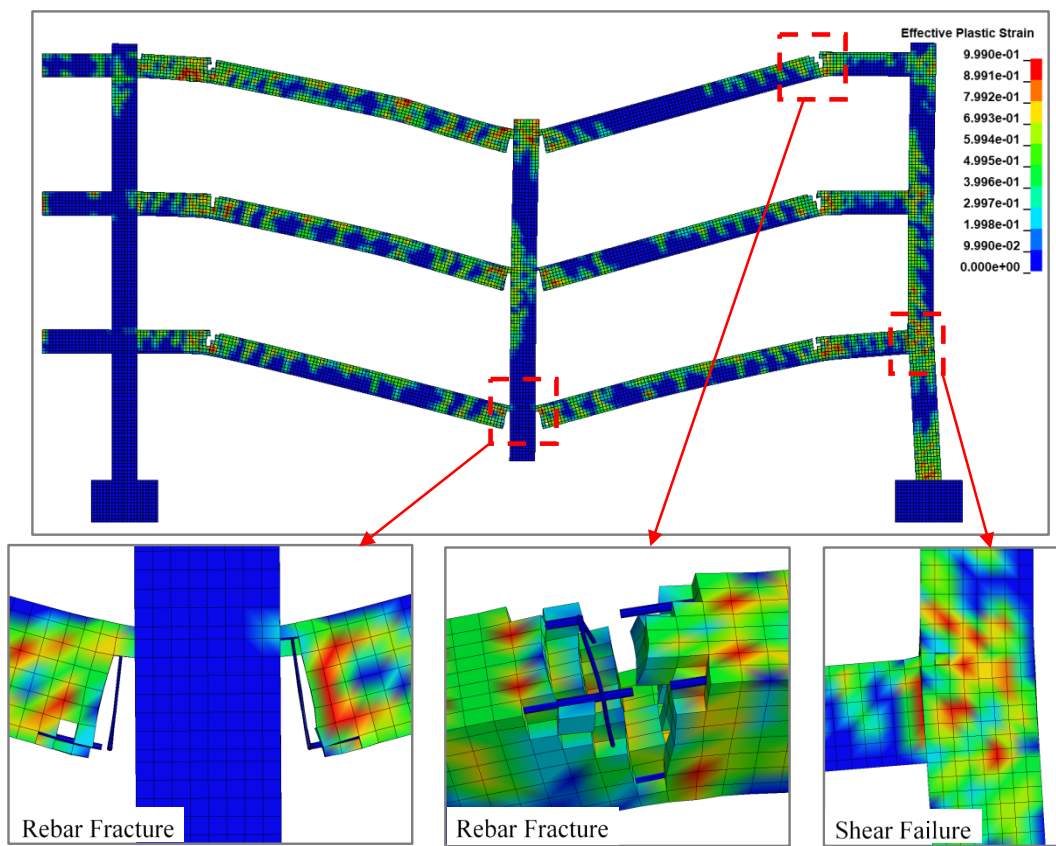
**Fig. 9**—Comparison of the horizontal movement response from numerical and test: (a) BFS, (b) BFL



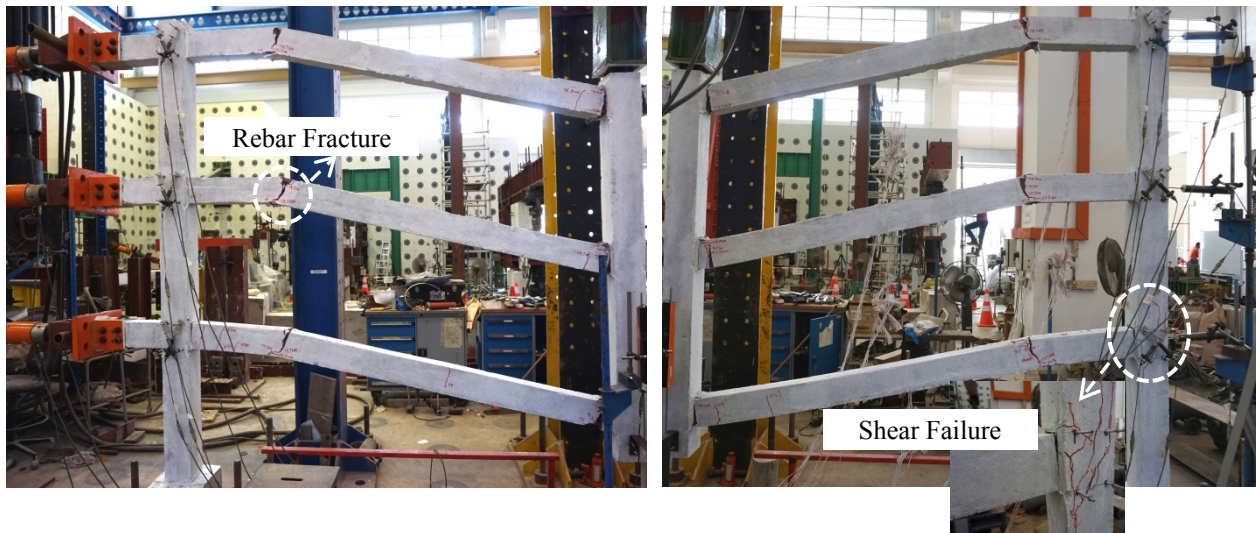
(a)



(b)  
**Fig. 10**—Comparisons of failure mode of BFS: (a) FEM, (b) Test



(a)



(b)  
**Fig. 11**–Comparisons of failure mode of BFL: (a) FEM, (b) Test

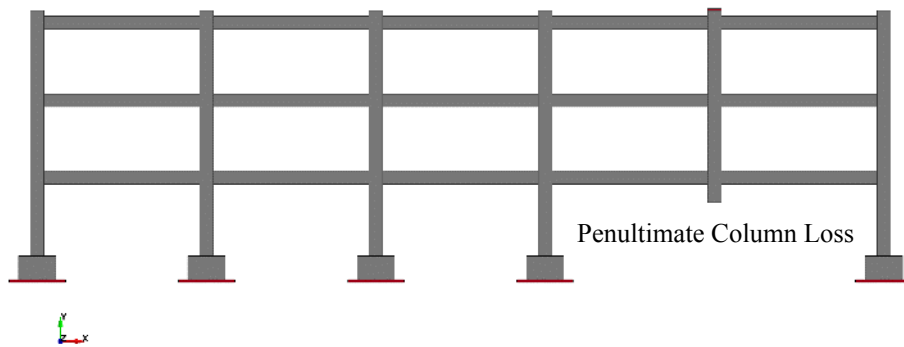
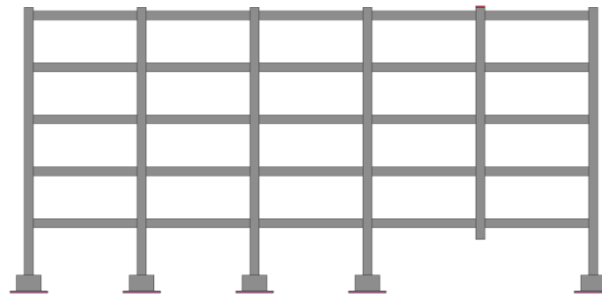
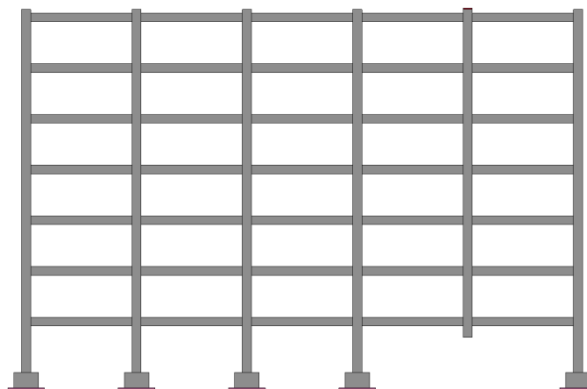


**Fig. 12**–Numerical model of BFS-P

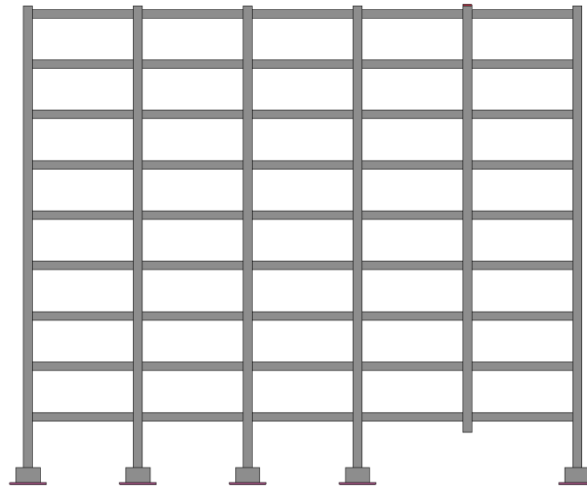


(a)



1

(b)



(c)

**Fig. 13**–Numerical models of number of different floors: (a) BFS-P-5F, (b) BFS-P-7F, (c) BFS-P-9F

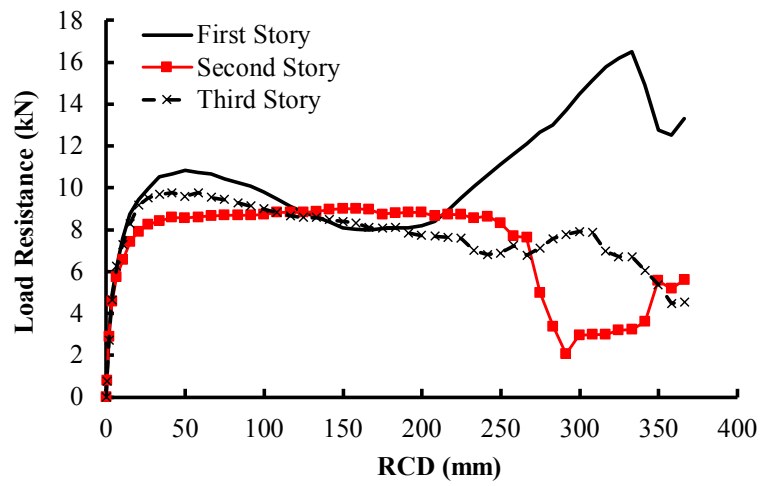


**Fig. 14**–Load resistance of each story of BFS-P

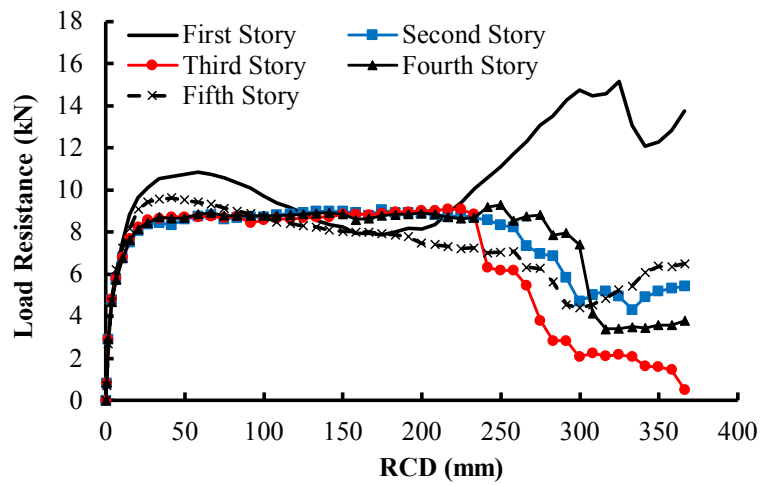


**Fig. 15**–Load resistance of each story of BFS-P-5F

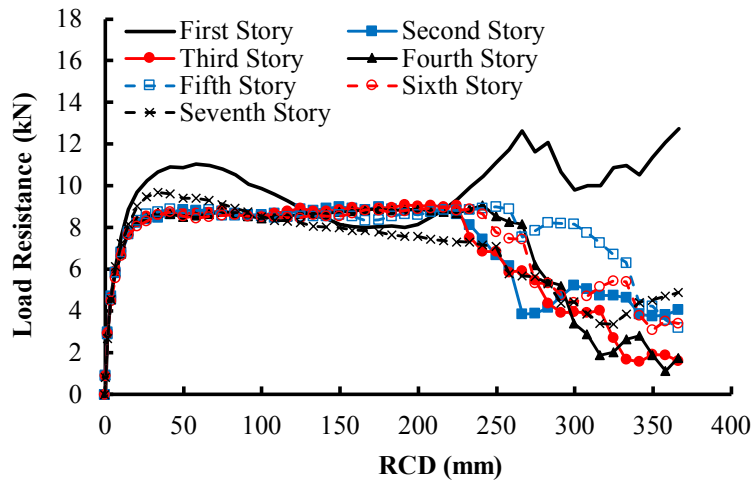


**Fig. 16**–Load resistance of each story of BFS-P-7F

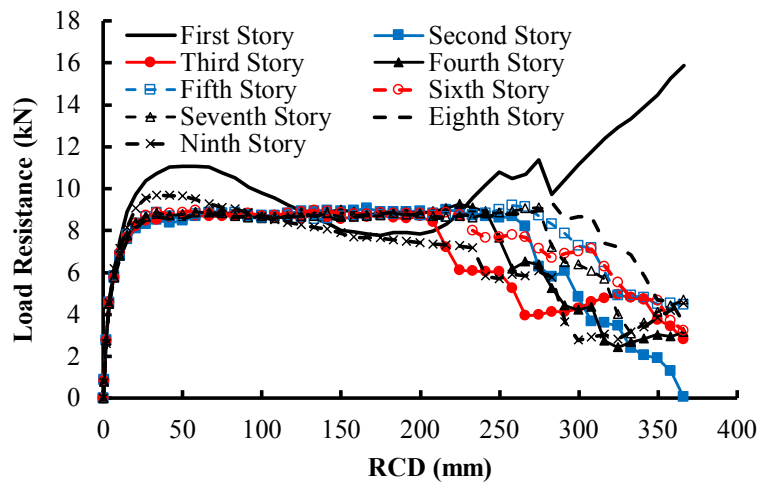
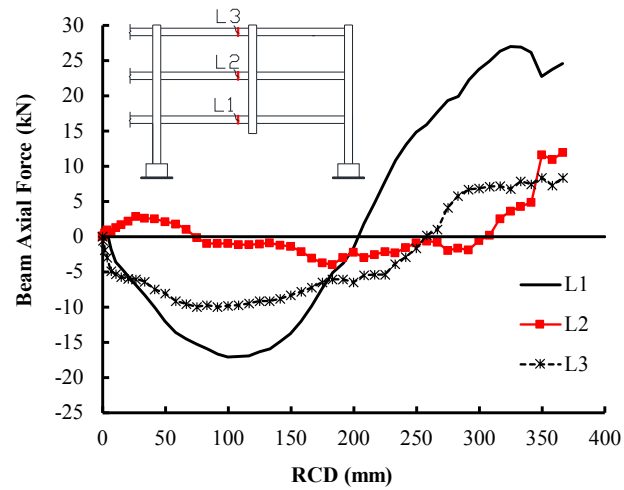
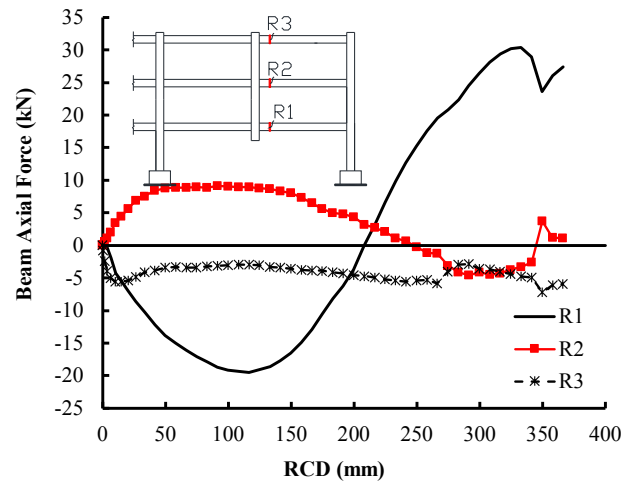


**Fig. 17**–Load resistance of each story of BFS-P-9F

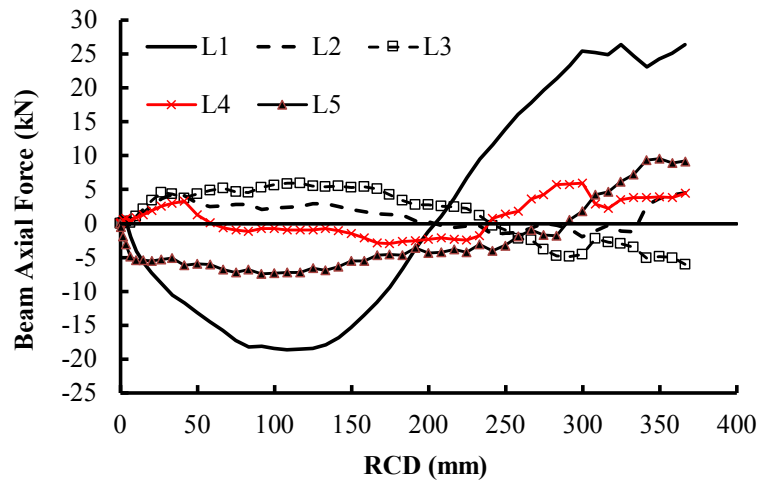


(a)

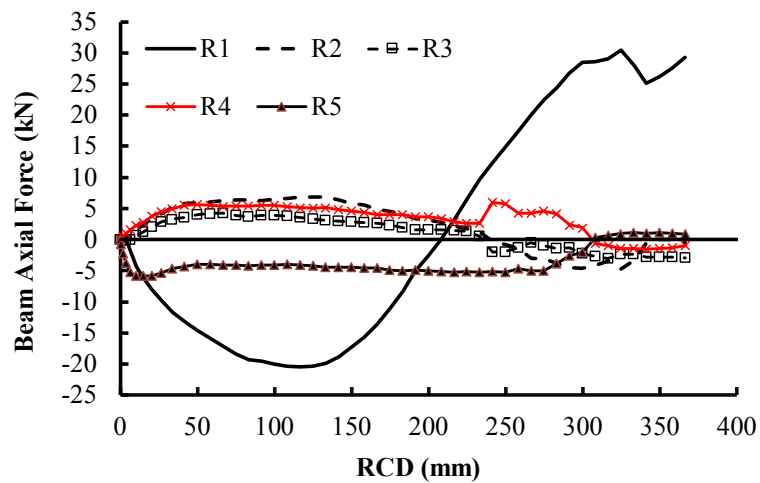


(b)

**Fig. 18**–Varying of beam axial forces of BFS-P: (a) left side of removed column, (b) right side of removed column

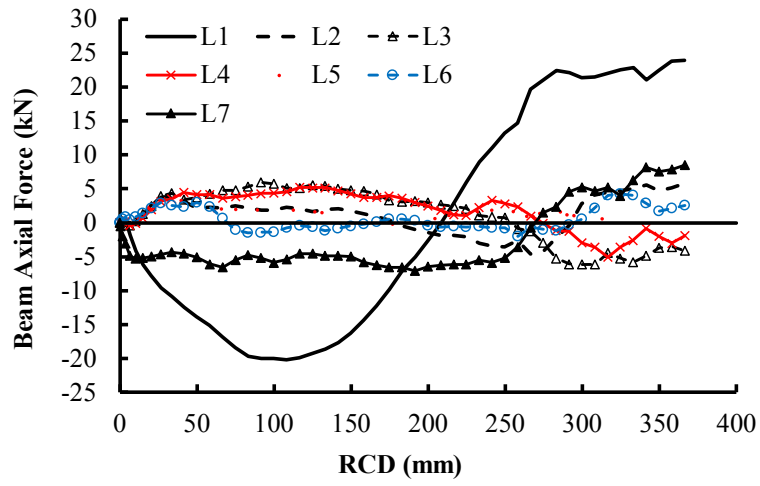


(a)

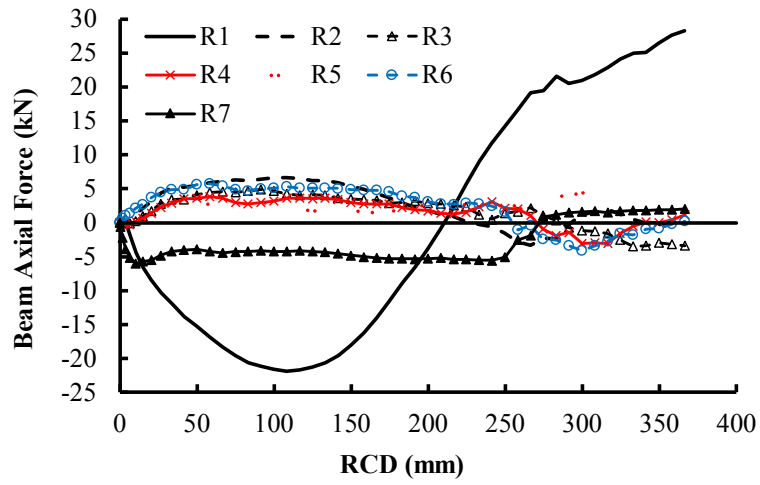


(b)

**Fig. 19**–Varying of beam axial forces of BFS-P-5F: (a) left side of removed column, (b) right side of removed column

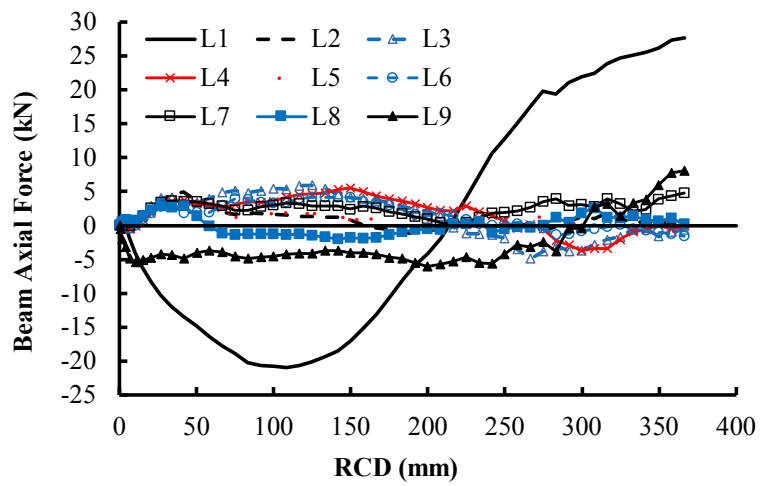


(a)

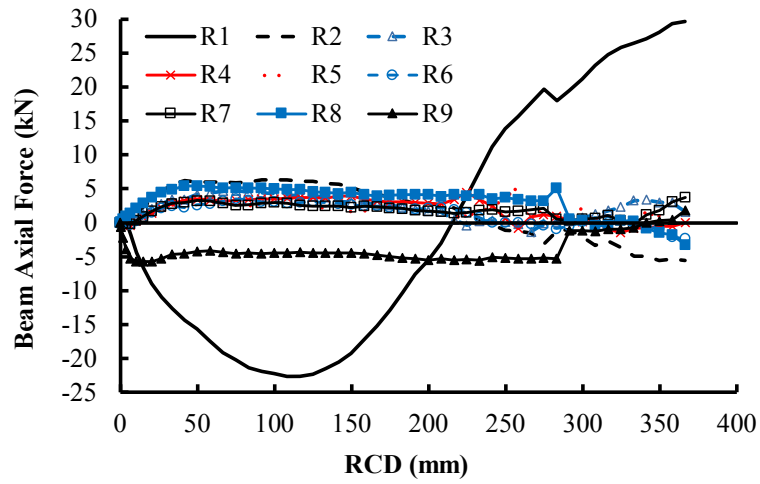


(b)

**Fig. 20**—Varying of beam axial forces of BFS-P-7F: (a) left side of removed column, (b) right side of removed column

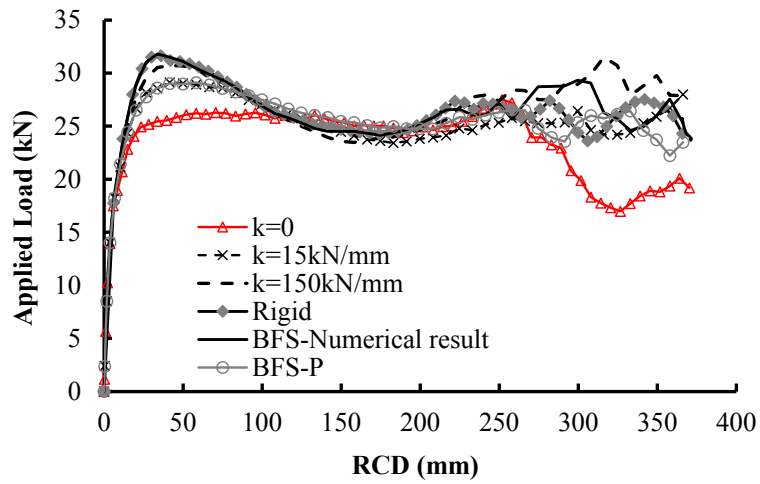


(a)

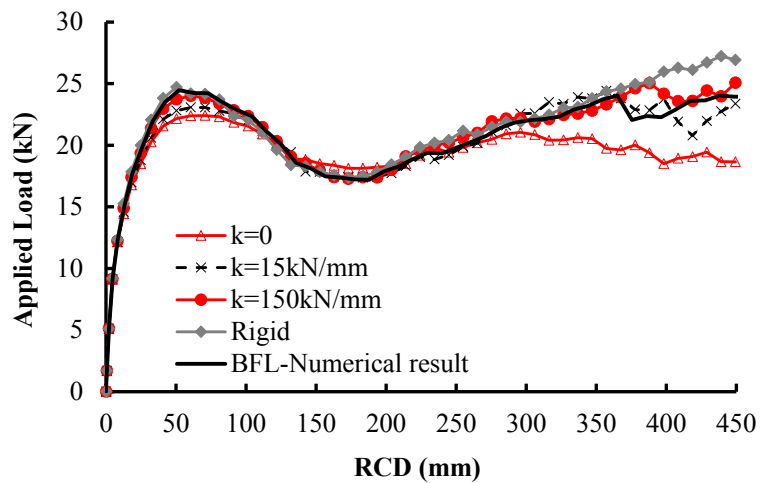


(b)

**Fig. 21**—Varying of beam axial forces of BFS-P-9F: (a) left side of removed column, (b) right side of removed column

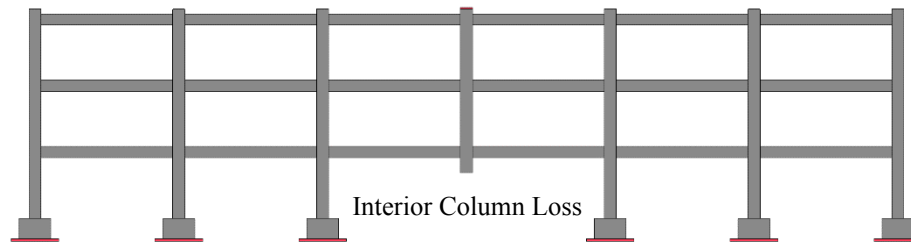


(a)

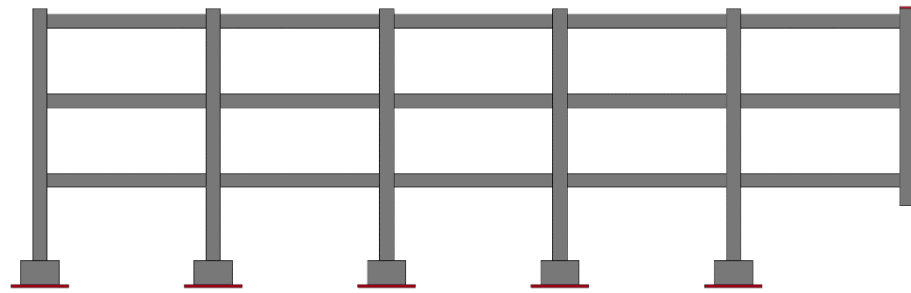


(b)

**Fig. 22**—Effects of horizontal stiffness of the constraints: (a) BFS, (b) BFL



(a)



(b)

**Fig. 23**–Numerical models of different column loss: (a) BFS-I, (b) BFS-C

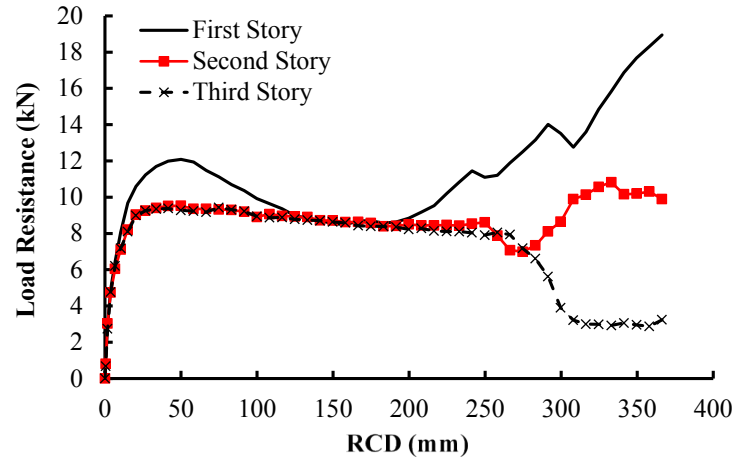


**Fig. 24**–Load resistance of each story of BFS-I

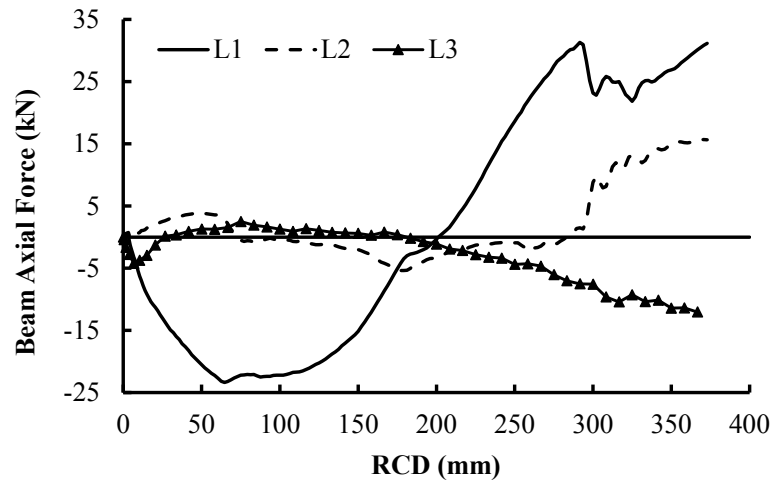


**Fig. 25**–Varying of axial force of the beams in different story of BFS-I

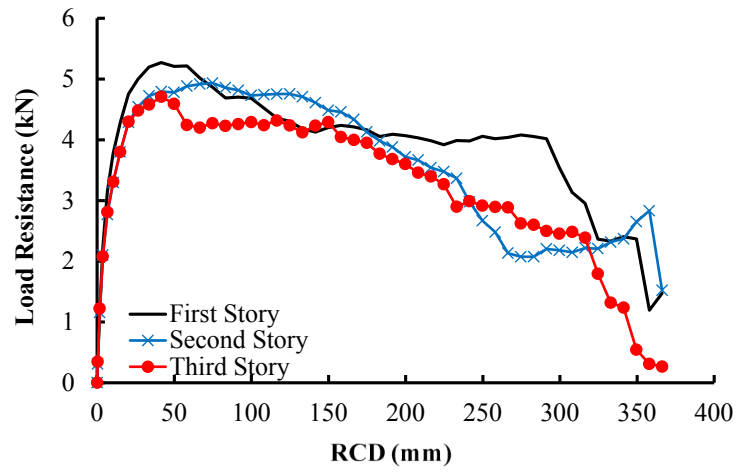


**Fig. 26**–Load resistance of each story of BFS-C

### **Research Highlights**

- Multi-storey RC frame was utilized to validate the FE model
- Load resisting mechanisms of each floor in a multi-storey frame is different
- The first storey achieved the largest compressive arch action and catenary action
- The horizontal constraints from surrounding bays is different to rigid constraints

# Numerical Evaluation of the Reliability of Using Single-Story Substructures to Study Progressive Collapse Behaviour of Multi-Story RC Frames

Kai Qian<sup>1\*</sup>, Yun-Hao Weng<sup>1</sup>, Feng Fu<sup>2</sup>, and Xiao-Fang Deng<sup>1</sup>

<sup>1</sup>College of Civil Engineering and Architecture, Guangxi University, 100 Daxue Road, China, 530004.

<sup>2</sup> School of Mathematics, Computer Science and Engineering, City, University of London, U.K.

**Abstract:** Progressive collapse is a global failure for a multi-story building. All stories above the removed column will consequently deform and help redistribute the loads initially withstood by the removed column. However, due to cost and excessive time to be involved, the majority of existing experimental researches regarding progressive collapse rely on single-story beam-column substructures or sub-assemblages. To date, how to use the results from single-story substructures or sub-assemblages to fully or confidently study the behavior of multi-story building is still unclear. Thus, it is imperative to investigate the relationship between the results of single-story substructures and the real behavior of multi-story buildings. Thus, for this purpose, in the present study, a series of planar multi-story reinforced concrete (RC) beam-column substructures were modeled using high-fidelity finite element software LS-DYNA. Firstly, the numerical models were validated by the test results of two three-story planar substructures with different design spans. Secondly, the validated models were explored on various load resistance of each story in the investigated multi-story frame. In addition, the effects of boundary conditions, missing column locations, story numbers on the variation of load resistance were studied in detail using the models.

**Keywords:** Progressive collapse; Multi-Story RC frames; Load transfer mechanism; Numerical simulations; Column removal scenario

\* Corresponding author. E-mail address: [qiankai@gxu.edu.cn](mailto:qiankai@gxu.edu.cn)

## 1. Introduction

Progressive collapse is defined in ASCE/SEI 7 [1] as “the spread of an initial local failure from element to element, eventually resulting in the collapse of an entire structure or a disproportionately large part of it”. To date, there are two main methods to design buildings to mitigate progressive collapse: direct and indirect design methods. For the indirect design method, integrity, redundancy, ductility, and minimum tie-force are required. However, when local damages are triggered, it is difficult to quantitatively evaluate the capacity and behavior of remaining building in resisting progressive collapse based on this method. For the direct design method, alternative load path method is most commonly used as it is event-independent. To understand the behavior of multi-story buildings subjected to sudden column missing scenario, Sasani et al. [2] carried out an on-site test for an actual 10-story reinforced concrete building following the explosive damage of an exterior column. Similarly, a six-story RC infilled-frame building was evaluated following the removal of two adjacent exterior columns simultaneously by Sasani [3]. Song et al. [4] tested a steel frame building subjected to physically removal of four ground columns from one of the perimeter frames to study the load redistribution of the building after each column removal. However, as the service load (live load and partial dead load) was removed prior to on-situ tests, the measured displacement response was little. Majority of on-situ tests only experienced elastic response. The plastic behavior especially for compressive arch action (CAA) and tensile catenary action (TCA) could not be captured and therefore be evaluated in detail. Thus, the majority of existing tests in laboratory regarding progressive collapse were single-story beam-column substructures based on alternative load path method (relied on push-down loading regime). A number of tests [5-13] quantified the effects of geometric characteristic and reinforcing details on the mobilization of CAA and TCA for progressive collapse prevention. It was found that the span/depth ratio has great effects on the mobilization of CAA when the RC frame

121  
122  
123 1 subjected to the loss of a middle column scenario. In addition, the CAA capacity is sensitive to the  
124  
125 2 horizontal stiffness provided by the beam ends. However, the amount of longitudinal reinforcements in  
126  
127 3 the structural concrete members has little effect on developing CAA. The researchers [8] indicated that  
128  
129  
130 4 the continuous top longitudinal reinforcements contributed to TCA capacity while Yi et al. [14]  
131  
132 5 indicated that both top and bottom longitudinal reinforcements provided contributed to TCA capacity.  
133  
134

135 6 Moreover, several studies [15-17] were carried out to evaluate the dynamic response and dynamic  
136  
137 7 load increase factor of RC beam-column sub-assemblages subjected to sudden column removal  
138  
139 8 scenario. Qian and Li [15] indicated that the acceleration of the frame after sudden column removal  
140  
141  
142 9 could be as large as 3.5g, where g is the acceleration of gravity, and the dynamic load increase factor  
143  
144 10 could be less than 1.38. Qian and Li [16] quantified the slab effects on the dynamic response of RC  
145  
146 11 frames subjected to the sudden removal of a ground corner column. In addition, they proposed an  
147  
148 12 equivalent single-degree-of-freedom (SDOF) model to predict the dynamic ultimate load capacity of  
149  
150 13 the tested specimens. The dynamic load increase factor of tested specimens was ranged from 1.30 to  
151  
152 14 1.34. Liu et al. [17] investigated the dynamic behavior of steel frames with different connections  
153  
154 15 subjected to sudden removal of a center column experimentally. The test results indicated that the  
155  
156 16 dynamic phenomenon may detriment the behavior of steel connections and degrade the progressive  
157  
158 17 collapse resistance of the substructures.  
159  
160  
161  
162

163 18 However, the reliability of using single-story substructures to study the behavior of multi-story  
164  
165 19 buildings is based on the assumption that the stories above the removed column have identical  
166  
167 20 performance, which is questionable and has not been proved. Weng et al. [18] used high fidelity finite  
168  
169 21 element (FE) models to investigate the load resisting mechanisms of each story for a multi-story flat  
170  
171 22 slab structure under a middle column loss scenario. The numerical results indicated that the load  
172  
173 23 resistance from each story in a multi-story flat slab building was different and the largest load resisting  
174  
175  
176  
177  
178  
179  
180

capacity occurred in the first story. However, for a multi-story RC frame, it may be different to flat slab structures as beams could help to redistribute the loads. In Qian and Li [19], two multi-story frames were tested based on displacement-controlled push-down method. As it is not feasible to test a multi-story frame to assess the load resisting contribution of each story, FE models, which are validated against the experimental tests, are used for deeper understanding of the various load transfer mechanism and load resisting contribution of each floor consequently. Moreover, the effects of the number of stories, boundary conditions, and missing column locations are also studied using the validated numerical models.

## 2. Previous Experimental Work

A quasi-static experimental study on progressive collapse resistance of planar RC beam-column substructures subjected to push-down loading regimes was conducted by Qian and Li [19] and the test results of two bare frames are used to validate the reliability of FE models in this numerical study. These two specimens (BFS and BFL) were one-quarter scaled. They were assumed to be subjected to the loss of a penultimate column. The dimension and reinforcement details of Specimen BFS are shown in Fig. 1. As can be seen in the figure, the beam span was 1800 mm. The story height was 900 mm in the first story and 825 mm in upper stories. The cross section of the beam and column was 90 mm×140 mm and 150 mm×150 mm, respectively. The concrete clear cover was 7 mm and 10 mm for beam and column, respectively. Enlarged foundation base with a size of 400 mm×300 mm was designed at the toe of side columns for fixing. The hoop stirrups with 90 degrees bends were utilized for transverse reinforcements. As it was non-seismically designed, no transverse reinforcements were placed in the joint region. The curtailment of longitudinal reinforcements in the beam was in accordance with Singapore Code CP-65 [20]. The middle column in ground level is assumed removed before test and thus, the middle column was only fabricated the upper two stories. For Specimen BFL,

similar reinforcement details and dimensions to Specimen BFS were used except longer span of 2400 mm designed. Average cylinder compressive strength measured on the days of testing for both specimens was 32.1 MPa. The yield strength of R3, R6, and T10 were 417 MPa, 449 MPa, and 515 MPa, respectively. The ultimate strength of R3, R6, and T10 were 479 MPa, 537 MPa, and 594 MPa. The measured elongation ratio of R3, R6, and T10 were 9.7 %, 13.3 %, and 16.9 %, respectively. “R” represents plain reinforcement while “T” represents deformed reinforcement.

The typical experimental setup and locations of instrumentations are shown in Fig. 2. As shown in the figure, the specimens were fixed to the strong floor by the foundation bases, which were cast monolithically with the side columns. A steel column and a specially designed steel assembly were installed to avoid unforeseen out-of-plane movement of the specimen. This specially designed steel assembly only allows vertical movement of the middle column through constraining its rotational and horizontal movements. A hydraulic jack with a 600 mm stroke was installed on the steel column to apply vertical load. It should be noted that the displacement-controlled push-down loading method was adopted in the reference tests [19]. A load cell was installed above the hydraulic jack to measure the applied vertical load. A roller together with a tension/compression load cell was installed horizontally at each extension part of the specimen to simulate the horizontal constraints of the beams in the surrounding bay.

### 3. Numerical Model Development and Validation

To illustrate the variation of load resisting capacity and mechanisms of the beams in different stores overtly, explicit solver software LS-DYNA [21] was used to build the FE models due to its numerical stability and various constitutive models available. The FE models were validated based on the experimental results first. As shown in Fig. 3, similar boundary conditions as experimental tests were used at the FE models. As gaps were deliberately left near the horizontal constraints for the

facility of installation, springs were installed horizontally at the beam ends of the extension part. The stiffness of the spring was determined by the measured horizontal reaction force and horizontal movements at the ends, which was roughly equal to 80 kN/mm at each beam end with a total of 240 kN/mm.

### ***3.1 Element types***

Fig. 3 shows the numerical model of Specimen BFS. Concrete is simulated by 8-node solid elements with reduced integration scheme. This solid formulation only has one integration point in each element, which can enhance computational efficiency with the promise of sufficient accuracy, but hourglass control should be defined properly when this type of element was adopted. Moreover, reinforcing bars were modeled using 2-node Hughes-Liu beam elements with 2×2 Gauss quadrature integration at the cross-section. This beam formulation can simulate the behavior of axial force, bi-axial bending, and finite transverse shear strains [22]. Furthermore, the rigid plates for supports or loading points were also modeled by 8-node solid elements and the springs for horizontal restraints were simulated by discrete elements.

### ***3.2 Bond-slip relationship simulation***

To improve the accuracy of modeling, considering the bond-slip relationship between reinforcement and concrete is important, as the perfect bonding assumption used in other models will cause over-prediction of load-carrying capacity and lead to premature fracture of reinforcement due to stress concentration [23]. In this numerical study, the bond-slip relationship between reinforcement and concrete material was considered by using keyword \*CONTACT\_1D to define one-dimensional

contact interface between the concrete and rebar elements. Virtual springs are defined between the slave nodes from beam elements and the master nodes from solid elements, and the spring force depends on relative displacements between the slave and master nodes [21]. However, simulating bond-slip behavior for all reinforcements would be complicated and required more computational resources. Based on test results, it was noted that the slip occurred mainly at the beam-column joints and the curtail point of top beam longitudinal reinforcements. As a result, similar to previous studies [24, 25], the CONTACT\_1D function was only used for the beam longitudinal reinforcements at the location of beam-column joints and the reinforcements near curtail points, as shown in Fig. 3. Besides, the remaining reinforcements were assumed to be perfect bonding to concrete using keyword \*Constrained\_Lagrange\_In\_Solid. To calibrate the properties of Contact\_1D, the bond-slip relationship proposed by fib Model Code 2010 [26] was applied. For monotonic loading, the bond stress  $\tau_b$  between concrete and hot-rolled plain bar for pull-out failure can be calculated as following [26]:

$$\begin{cases} \tau_b = \tau_{b\max} (s / s_1)^{0.5} & \text{for } 0 \leq s \leq s_1 \\ \tau_b = \tau_{b\max} = 0.3\sqrt{f_c} & \text{for } s > s_1 \end{cases} \quad (1)$$

Where  $s_1 = 0.1$  mm;  $f_c$  is standard cylinder compressive strength. In the tests, the compressive strength of concrete is 32.1 Mpa. Therefore,  $\tau_{b\max} = 1.70 \text{ MPa}$ .

For the CONTACT\_1D (LS-DYNA) function [21], the bonding relationship between the beam elements and solid elements is assumed to be elastic-perfectly-plastic. After elastic stage, the bond stress would decay following an exponential damage curve. The constitutive law of shear stress  $\tau$  and slip  $s$  is given as [21]:

$$\begin{cases} \tau = G_s s & \text{for } s \leq s_{\max} \\ \tau = \tau_{\max} e^{-h_{\text{dmg}} D} & \text{for } s > s_{\max} \end{cases} \quad (2)$$

where  $G_s$  is bond shear modulus;  $s_{\max}$  is maximum elastic slip;  $h_{\text{dmg}}$  is damage curve exponential coefficient;  $D$  is damage parameter, which is equals  $(s-s_{\max})$ .

The comparison between Eqs. (1) and (2) indicates that the values of  $h_{\text{dmg}}$  and  $\tau_{\max}$  are equal to 0 and 1.7 Mpa, respectively. Based on the suggestion from Pham et al. [24] and Yu et al. [25],  $s_{\max} = 0.5 s_I = 0.05$  mm. Therefore,  $G_s = \tau_{\max} / s_{\max} = 34 \text{ MPa} / \text{mm}$ . The comparison of the bond-slip relationship between the fib Model Code 2010 [26] and the suitable model used in CONTACT\_1D is shown in Fig. 4.

### 3.3 Material model

In this study, Continuous surface cap model (CSCM) is chosen to simulate concrete material. This model can effectively model damage-based softening and modulus reduction, shear dilation, shear compaction, confinement effect, and strain rate effect under low constraint conditions [27]. Previous studies had proven its accuracy in the simulation of RC components under both quasi-static and dynamic conditions [24, 25, 28].

The CSCM provides a simplified version (\*Mat\_CSCM\_CONCRETE) for concrete materials with the compressive strength between 28 Mpa and 48 Mpa. The default parameters depend on three input parameters: unconfined compressive strength  $f'_c$ , maximum aggregate size  $A_g$ , and units. For both Specimens BFS and BFL,  $f'_c$  and  $A_g$  are 32.1 Mpa and 8 mm, respectively. The CSCM also provides a strain-based approach of erosion algorithm to simulate material failure, and the related parameter is “ERODE”. When the “ERODE” is set greater than 1.0, the concrete elements would be deleted if damage index exceeds 0.99 and the maximum principal strain exceeds (ERODE-1.0) according to LS-DYNA keyword user’s manual [21]. This feature is used here to effectively model the failure mode of the frame. In the reference test results, the failure modes of the multi-story frames were governed by

the flexure and tensile actions, primarily denoted by the formation of severe cracks at the beam ends near the center column and at the curtail points of beam top longitudinal reinforcements. Therefore, the maximum principal strain is a suitable criterion for erosion algorithm. The value of “ERODE” is mesh-dependent, and set as 1.10, corresponding to the maximum principal of 0.1, for element size 20 mm according to the previous work [24]. The strain rate effect of the CSCM is ignored because only quasi-static behavior is considered.

The isotropic elastic-plastic material model Mat\_Plastic\_Kinematic (MAT\_003) is used to model reinforcements. The elastic modulus, yield strength, tangential modulus after yielding, and ultimate strain is determined based on properties of steel bars. Also, the strain rate effect is excluded.

As choosing the appropriate mesh size is important to obtain reliable and effective results, mesh sensitivity is evaluated. Four different mesh sizes of elements (side length for solid elements and length for beam elements), including 30 mm, 25 mm, 20 mm, and 15 mm, were employed for Specimen BFS. The results of the load-removed column displacement (RCD) relationship for different mesh sizes are shown in Fig. 5. Obviously, mesh size of 20 mm is adequate, as further mesh refinement is not able to cause any remarkable convergence but instead taking larger computational resources. As a result, the mesh size is chosen as 20 mm.

However, based on the default parameters of the CSCM, the numerical models will overestimate the initial stiffness and load resisting capacity of the specimens, as shown in Fig. 6. Unconfined uniaxial stress-strain relationship for 32.1 MPa based on the default parameters of the CSCM is shown in Fig. 7. As can be seen from the figure, the compressive strength is attained at a strain of 0.001. But in reality, when normal strength concrete reaches its compressive strength, the strain is usually at about 0.002. Therefore, the elastic modulus of concrete should be reduced properly to improve the numerical results, which had been pointed out by Yu et al. [25]. On the other hand, Yu et al. [25, 28] suggested

that the tensile fracture energy  $G_{ft}$  could be reduced to 80 % of the default one when the simulating result is over predicted. If shear or compressive based damage is significant, then setting  $G_{fs}$  (compressive fracture energy) = 0.5  $G_{ft}$  and  $G_{fc}$  (shear fracture energy) = 50  $G_{ft}$  is reasonable [25]. However, the default ones are assumed as  $G_{fs}=G_{ft}$  and  $G_{fc}=100G_{ft}$ . Since severe shear cracks were formed in the exterior joint in the first floor and the concrete crushing was not obvious during testing, only the reduced shear fracture energy is used for the CSCM model herein. The user-specified material property inputs for CSCM are listed in Table 1. When the adjusted material property is used for simulating, the stiffness of the unconfined uniaxial compression is lower than that of the default one and the compressive stress reduces faster in the softening stage, as shown in Fig. 7. However, the adjusted material property can improve the numerical results significantly, as shown in Fig. 6. Therefore, these adjustments are finally used to simulate Specimens BFS and BFL.

### 3.4 Verification of numerical model

Fig. 8 shows the comparison of load-displacement curves from numerical simulation and experimental results. Generally, the FE models can simulate all three stages of the structural responses well. In the first stage, the structural resistance increases until reaching the first peak load. The resistance is attributed into the flexural action and compressive arch action (CAA). Then, the resistance decreases due to the weakening of CAA in the second stage. In the last stage, the resistance increases again due to the development of tensile catenary action (TCA), and abrupt reduction since rebar fracture was also simulated. For Specimens BFS and BFL, the error between the predicted and measured peak capacity is less than 10 %, as shown in Fig. 8.

Fig. 9 shows the comparison of the simulated and measured horizontal displacement responses at exterior joints. In general, the FE models could predict the horizontal movements of the joints well

including the inward and outward movements and transition phase. In CSCM, the contour plot of effective plastic strain could indirectly reflect the crack pattern of the specimens as the crack pattern could not be physically displayed in LS-DYNA [24]. Figs. 10 and 11 compare the failure modes of test specimens from numerical simulations and experimental results. In general, the FE models could simulate the failure modes and crack patterns well including the positions of rebar fracture and concrete spalling. Therefore, the validated FE models were utilized to further study the effects of boundary conditions, locations of column missing, and story numbers on the varying load transfer mechanism in floors.

## **4. Detailed Discussion of the Numerical Results**

### ***4.1 Load transfer mechanisms of planar multi-story RC frames***

As mentioned above, most of the existing tests on progressive collapse research are single-story beam-column substructures or sub-assemblages due to cost and time consideration. However, progressive collapse is a global behavior for a multi-story building, and the load transfer mechanisms may not be the same in each story, especially for the asymmetric structure. Therefore, it is necessary to investigate the various load transfer mechanisms of each floor of the frame model. However, the horizontal constraints of the test specimens were simplified due to the limitation of the cast and testing space. Therefore, to get a more realistic response of structures, a five-span planar frame model with penultimate column loss named BFS-P was built based on the verified modeling techniques in BFS, as shown in Fig. 12. Comparing to BFS, BFS-P has a close-to-reality boundary condition provided by the beams in surrounding bay. Therefore, BFS-P could be the key reference model in this numerical simulation program. To understand the effect of story numbers on the load transfer mechanism of planar RC beam-column substructures subjected to progressive collapse, BFS-P-5F with five stories,

BFS-P-7F with seven stories, and BFS-P-9F with nine stories were also modeled based on the model BFS-P, as shown in Fig. 13.

#### ***4.2 Structural resistance of each story***

The structural resistance of each story equals the summation of vertical loads on both sides of the beam section located above the removed column. Fig. 14 illustrates the load resistance of each story in specimen BFS-P. As shown in the figure, the load resistance of each story is different after elastic stage. It can be seen that the first story contributed the greatest load resistance when the RCD is less than 133 mm or larger than 220 mm. In terms of CAA capacity, the resistance from the third story is larger than that of the second story and the biggest one is measured in the first story. Regarding the TCA stage, the biggest TCA capacity is also measured in the first story. In general, the assumption of each story demonstrating the same load transfer mechanisms and resistance, which is the basic assumption to use the behavior of a single-story substructure to represent a real multi-story frame, is not accurate for planar frames subjected to a penultimate column missing scenario.

Figs. 15, 16, and 17 show the story resistance results of BFS-P-5F, BFS-P-7F, and BFS-P-9F, respectively. Similar to BFS-P, the story resistance began diverging after the elastic stage, and the resistance of the first story is larger than the ones of other stories when the RCD is less than 133 mm or greater than 216 mm. Besides, prior to the fracture of longitudinal reinforcements, the load resistance of the middle stories is quite similar, indicating that the middle stories have similar load transfer mechanisms. To reveal the behavior of multi-story frame subjected to the loss of a column scenario, commonly utilized single-story sub-assembly tests may be insufficient. To the contrary, three sub-assembly tests (top story, one of middle story, and ground story) with proper boundary conditions were required.

### 4.3 Development of axial forces in beams

To reveal the difference of load transfer mechanism of the beams in each story, the results of the beam axial force of BFS-P were also extracted and presented in Fig. 18. As the axial force throughout each beam is identical, the development of the axial force of the whole beam can be represented by that of one arbitrary section at the beam. Due to asymmetry, the axial force of the beams at different sides of the removed column may be different. Therefore, the axial forces of the beam sections, which are at a distance of 200 mm away from the beam-column interface, were extracted. The labels of L1 to L3 represent the sections at the left side of the removed column (called interior bay) while the labels of R1 to R3 represent the sections at the right side of the removed column (called exterior bay).

In elastic stage, the beams in the first and second stories are in tension while the beam in third story is in compression. These beams worked like a large composite beam under flexure. After elastic stage, as shown in Fig. 18a, the interior-bay beam in the first story (IB-beam-1<sup>st</sup>) begins to develop compressive force initially and achieved the maximum compressive force of -17.0 kN at a RCD of 108 mm. After that, the axial force of the IB-beam-1<sup>st</sup> starts to decrease, and changes into tension at a RCD of 208 mm. Different from the IB-beam-1<sup>st</sup>, the axial force of the interior-bay beam in the second story (IB-beam-2<sup>nd</sup>) is in tension initially, and it transfers to compression at a RCD of 74 mm. The maximum compressive force of the IB-beam-2<sup>nd</sup> is -4.0 kN, which is only 23.5 % of the one of the IB-beam-1<sup>st</sup>. Moreover, the axial force of the IB-beam-2<sup>nd</sup> transfers to tension again at a RCD of 308 mm. For the interior-bay beam in the third story (IB-beam-3<sup>rd</sup>), the beam is in compression until the RCD reaches 266 mm, and the maximum compressive force is -10.0 kN, which is 58.8 % of the one of the IB-beam-1<sup>st</sup>. Besides, the maximum tensile forces of IB-beam-1<sup>st</sup>, IB-beam-2<sup>st</sup>, and IB-beam-3<sup>st</sup> are 27.0 kN, 11.9 kN, and 8.4 kN, respectively. For the exterior bay, as shown in Fig. 18b, the

development of the axial force of the exterior-bay beam in the first story (EB-beam-1<sup>st</sup>) is quite similar to the one of the IB-beam-1<sup>st</sup>, which is in compression first and finally in tension. Due to interaction of the beam-column elements among stories, the exterior-bay beam in the second story (EB-beam-2<sup>st</sup>) is in tension first and in compression slight after RCD of 250 mm. However, the exterior-bay beam in third story (EB-beam-3<sup>rd</sup>) is always in compression during the whole loading history. In a word, the distributions of axial forces in both interior-bay and exterior-bay beams indicate the CAA could develop in the first and third stories, whereas flexural action is the main mechanism of second story to redistribute the gravity load. Moreover, the significant axial tensile forces of the IB-beam-1<sup>st</sup> and EB-beam-1<sup>st</sup> in the large deformation stage also illustrate the TCA could develop in the first story beams effectively.

Figs. 19, 20, and 21 show the development of the axial forces in the beams of different stories for BFS-P-5F, BFS-P-7F, and BFS-P-9F, respectively. It is observed that the beam axial forces in the middle stories is quite similar. Most of the beam axial forces in the middle stories are mainly in tension first, and the compressive force appears at large deflection stage, indicating that flexural action is the main mechanism of these stories to balance the gravity load. On the other hand, the beam axial forces of the top and bottom stories are similar to the ones of BFS-P. Similarly, the greatest compressive and tensile forces are measured in the first story, which indicates CAA and TCA can develop in the first story effectively. Further parametric study in Section 5.2 will evaluate the accuracy of the conclusion for the frames subjected to interior or corner removal scenarios.

## 5. Parametric Study on Planar Multi-Story RC Frame

### 5.1 Effect of boundary conditions

As shown in Fig. 2, in the referenced tests [19], the horizontal constraints of the beams in surrounding bay were simplified due to the limitation of the cast and testing space. However, the reliability of the simplification has not been evaluated properly. To quantify the effect of the horizontal restraint stiffness provided by the surrounding bay, four different horizontal restraint stiffness, including 0, 15 kN/mm, 150 kN/mm and rigid, were used for the models of BFS and BFL.

Fig. 22 shows the load-displacement curves of BFS and BFL with different boundary conditions. It should be noted that the results of tests are similar to that with rigid restraints for both Specimens BFS and BFL. As shown in Fig. 22, when the horizontal restraint stiffness decreases from rigid to 0, the first peak load (FPL) of BFS and BFL decreases to 87 % and 90 %, respectively, due to weakened CAA. However, reducing the horizontal restraint stiffness is not sensitive to the structural resistance at large deflection stage. Even though there are no spring restraints applied, both BFS and BFL can develop TCA in the initial stage. This is because the remaining two side columns can provide sufficient lateral stiffness to develop TCA initially. However, the TCA weakens due to damage of the side columns later.

As shown in Fig. 22a, the FPL of BFS-P, which has a more real boundary condition, is 92 % of that of the BFS. It means that the horizontal restraint stiffness used in the tests may be larger than the real one.

## 5.2 Effect of location of removed column

For the referenced tests [19], only the scenario of missing a penultimate column is investigated. Two extra numerical models, which were called BFS-I (an interior column was removed in advance) and BFS-C (a corner column was removed in advance), were built to investigate the effects of different column removal scenarios on the load transfer mechanism of each story, as shown in Fig. 23. Fig. 24 shows the decomposition of the load resistance of BFS-I. Similar to BFS-P, the first story achieves the highest initial stiffness and provides the majority of CAA and TCA capacity. However, different from BFS-P, the resistances of the second and third stories are almost the same before RCD reached 285 mm. The difference in the load resistance of these two stories is mainly due to the mobilization of TCA in the second story. As shown in Fig. 25, when RCD exceeds 285 mm, the beams of the second story start to be in tension, indicating the TCA starts to develop in second story too.

For BFS-C, as shown in Fig. 26, the FPL of the first story is also the largest among stories. However, the second story achieves the second largest one, which is different to BFS-P and BFS-I. The different resistance mechanism is due to interaction of the beam-column elements among stories (Vierendeel action).

## 6. Conclusions

Based on the numerical and parametric studies conducted in this study, the following conclusions are drawn:

1. Comparing with experimental results, it is found that high fidelity numerical models are able to accurately simulate the global behavior of the planar multi-story RC frame subjected to a penultimate column loss scenario.

2. For a planar multi-story RC frame subjected to a penultimate column removal scenario, the

load transfer mechanism of each story is not identical. However, when increasing the number of stories, it can be found that the load transfer mechanism of the middle stories is almost the same. Therefore, the behavior of a planar multi-story frame should be equivalently investigated by three types of single-story beam-column assemblies (top-story, middle-story, and ground-story) with proper boundary conditions.

3. Horizontal restraint stiffness can significantly affect the development of CAA. Reducing the restraint stiffness of the horizontal springs would decrease the FPL of the frames due to the weakening of CAA. When the horizontal restraint stiffness decreases from rigid to 0, the FPL of BFS and BFL decreases by 87 % and 90 %, respectively. However, horizontal restraint stiffness affecting is insensitive to the development of TCA. Even though spring restraint stiffness reduces to 0, the rest of side columns can provide enough constraints to develop TCA partially.

4. It is found from the comparison of the load-displacement curves between the specimens BFS-P and BFS that the load capacity of the Specimen BFS-P is relatively less than that of the Specimen BFS. It means that the horizontal constraints applied on the tests may be stronger than the real one, which will overestimate the capacity of the structure to mitigate progressive collapse.

5. Numerical analysis on different column removal scenarios indicates that the beams from a planar multi-story RC frame subjected to progressive collapse demonstrate different load resistance. However, the beam in the first story achieves the greatest initial stiffness and load resisting capacity regardless of the location of removed column.

## Acknowledgments

The authors gratefully acknowledge the financial support provided by the Natural Science Foundation of China (Nos. 51778153, 51568004, 51478118). The high-level innovation team in

colleges and universities and excellence scholar program in Guangxi (201738). Any opinions, findings and conclusions expressed in this paper do not necessary reflect the view of Natural Science Foundation of China.

## References

- [1] ASCE/SEI 7. Recommendations for designing collapse-resistant structures. Structural Engineering Institute-American Society of Civil Engineers, 2010, Reston, VA.
- [2] M. Sasani, M. Bazan, S. Sagiroglu, Experimental and analytical progressive collapse evaluation of actual reinforced concrete structure, ACI Structural Journal 104(6) (2007) 731-739.
- [3] M. Sasani, Response of a reinforced concrete infilled-frame structure to removal of two adjacent columns, Engineering Structures 30(9) (2008) 2478-2491.
- [4] B.I. Song, K.A. Giriunas, H. Sezen, Progressive collapse testing and analysis of a steel frame building, Journal of Constructional Steel Research 94 (2014) 76-83.
- [5] Y.P. Su, Y. Tian, X.S. Song, Progressive collapse resistance of axially-restrained frame beams, ACI Structural Journal 106(5) (2009) 600-607.
- [6] M. Sasani, A. Werner, A. Kazemi, Bar fracture modeling in progressive collapse analysis of reinforced concrete structures, Engineering Structures 33(2) (2011) 401-409.
- [7] I. Azim, J. Yang, S. Bhatta, F. Wang, Q-F. Liu, Factors Influencing the progressive collapse resistance of RC frame Structures. Journal of Building Engineering, 2020; 27.
- [8] J. Yu, K.H. Tan, Experimental and numerical investigation on progressive collapse resistance of reinforced concrete beam column sub-assemblages, Engineering Structures 55 (2013) 90-106.
- [9] N. FarhangVesali, H. Valipour, B. Samali, S. Foster, Development of arching action in longitudinally-restrained reinforced concrete beams. Construction and Building Materials 47 (2013) 7-19.

- [10]K. Qian, B. Li, J.X. Ma, Load-carrying mechanism to resist progressive collapse of RC buildings, Journal of Structural Engineering 141(2) (2015) 04014107.
- [11]K. Qian, B. Li, Z. Zhang, Influence of multicolumn removal on the behavior of RC floors, Journal of Structural Engineering 142(5) (2016) 04016006.
- [12]P.Q. Ren, Y. Li, X.Z. Lu, H. Guan, Y.L. Zhou, Experimental investigation of progressive collapse resistance of one-way reinforced concrete beam-slab substructures under a middle-column-removal scenario, Engineering Structures 118 (2016) 28–40.
- [13]X.Z. Lu, K.Q. Li, C.F. Li, Y. Li, New analytical calculation models for compressive arch action in reinforced concrete structures, Engineering Structures 168 (2018) 721-735.
- [14]W.J. Yi, Q.F. He, Y. Xiao, S.K. Kunnath, Experimental study on progressive collapse-resistant behavior of reinforced concrete frame structures, ACI Structural Journal 105(4) (2008) 433-439.
- [15]K. Qian, B. Li, Dynamic performance of RC beam-column substructures under the scenario of the loss of a corner column-experimental results, Engineering Structures 42 (2012) 154-167.
- [16]K. Qian, B. Li, Quantification of slab influence on the dynamic performance of RC frames against progressive collapse, Journal of Performance of Constructed Facilities 29(1) (2015) 04014029.
- [17]C. Liu, K.H. Tan, T.C. Fung, Component-based steel beam-column connections modeling for dynamic progressive collapse analysis, Journal of Constructional Steel Research 107 (2015) 24-36.
- [18]Y.-H. Weng, K. Qian, F. Fu, Q. Fang, Numerical investigation on load redistribution capacity of flat slab substructures to resist progressive collapse, Journal of Building Engineering 29 (2020) 101109.
- [19]K. Qian, B. Li, Effects of masonry infill wall on the performance of RC frames to resist progressive collapse, Journal of Structural Engineering 143(9) (2017) 04017118.

- [20] CP 65. Structural use of concrete, part 1. Code of practice for design and construction. Singapore Standard, 1999.
- [21] J. Hallquist, LS-DYNA keyword user's manual, Version 971, Livermore Software Technology Corporation, 2007, Livermore, CA.
- [22] J. Hallquist, LS-DYNA theoretical manual. Livermore Software Technology Corporation, 1998, Livermore, CA.
- [23] Y. Bao, H.S. Lew, S.K. Kunnath, Modeling of reinforced concrete assemblies under column-removal scenario, Journal of Structural Engineering 140(1) (2014) 04013026.
- [24] A.T. Pham, K.H. Tan, J. Yu, Numerical investigations on static and dynamic responses of reinforced concrete sub-assemblages under progressive collapse, Engineering Structures 149 (2017) 2-20.
- [25] J. Yu, L. Luo, Y. Li, Numerical study of progressive collapse resistance of RC beam-slab substructures under perimeter column removal scenarios, Engineering Structures 159 (2018) 14-27.
- [26] Betonbau. Fib model code for concrete structures 2010. Ernst & Sohn 2013.
- [27] Y. Wu, J.E. Crawford, J.M. Magallanes, Performance of LS-DYNA concrete constitutive models, 12th Int. LS-DYNA Users Conf., Livermore Software Technology Corporation, 2012, Livermore, CA.
- [28] J. Yu, Y.P. Gan, J. Wu, H. Wu, Effect of concrete masonry infill walls on progressive collapse performance of reinforced concrete infilled frames, Engineering Structures 191 (2019) 179-193.

## Captions of tables

**Table 1-** Model parameters of CSCM after adjustment (Units: N, mm and ms)

## Captions of figures

**Fig. 1**–Reinforcement layout of the Specimen BFS: (a) Elevation view, (b) Cross section of RC frame

Note: Unit in mm, T=Deformed reinforcing bar; R=Plain reinforcing bar

- Fig. 2**–Test setup and instrumentation
- Fig. 3**–Numerical model of Specimen BFS
- Fig. 4**–Comparison of bond-slip relationship between Model Code 2010 and Contact\_1D
- Fig. 5**–Comparisons of different mesh sizes
- Fig. 6**–Comparisons of different concrete input parameters
- Fig. 7**–Unconfined uniaxial stress-strain relationship of concrete for 32.1 MPa based on CSCM
- Fig. 8**–Comparison of the load-displacement between simulation and test: (a) BFS, (b) BFL
- Fig. 9**– Comparison of the horizontal movement response from numerical and test: (a) BFS, (b) BFL
- Fig. 10**–Comparisons of damage patterns of BFS: (a) FEM, (b) Test
- Fig. 11**–Comparisons of damage patterns of BFL: (a) FEM, (b) Test
- Fig. 12**–Numerical model of BFS-P
- Fig. 13**–Numerical models of number of different floors: (a) BFS-P-5F, (b) BFS-P-7F, (c) BFS-P-9F
- Fig. 14**–Load resistance of each story of BFS-P
- Fig. 15**–Load resistance of each story of BFS-P-5F
- Fig. 16**–Load resistance of each story of BFS-P-7F
- Fig. 17**–Load resistance of each story of BFS-P-9F
- Fig. 18**–Development of beam axial forces of BFS-P: (a) Left side of removed column, (b) Right side of removed column
- Fig. 19**–Development of beam axial forces of BFS-P-5F: (a) Left side of removed column, (b) Right side of removed column
- Fig. 20**–Development of beam axial forces of BFS-P-7F: (a) Left side of removed column, (b) Right side of removed column
- Fig. 21**–Development of beam axial forces of BFS-P-9F: (a) Left side of removed column, (b) Right side of removed column
- Fig. 22**–Comparison of different boundary conditions: (a) BFS, (b) BFL,
- Fig. 23**–Numerical models of different column loss: (a) BFS-I, (b) BFS-C
- Fig. 24**–Load resistance of each story of BFS-I
- Fig. 25**–Development of beam axial forces of BFS-I
- Fig. 26**–Load resistance of each story of BFS-C

1261

1262

1263

1264

1265

1266

1267

1268

1269

1270

1271

1272

1273

1274

1275

1276

1277

1278

1279

1280

1281

1282

1283

1284

1285

1286

1287

1288

1289

1290

1291

1292

1293

1294

1295

1296

1297

1298

1299

1300

1301

1302

1303

1304

1305

1306

1307

1308

1309

1310

1311

1312

1313

1314

1315

1316

1317

1318

1319

1320

1

2

3

4

5

6

7

8

9

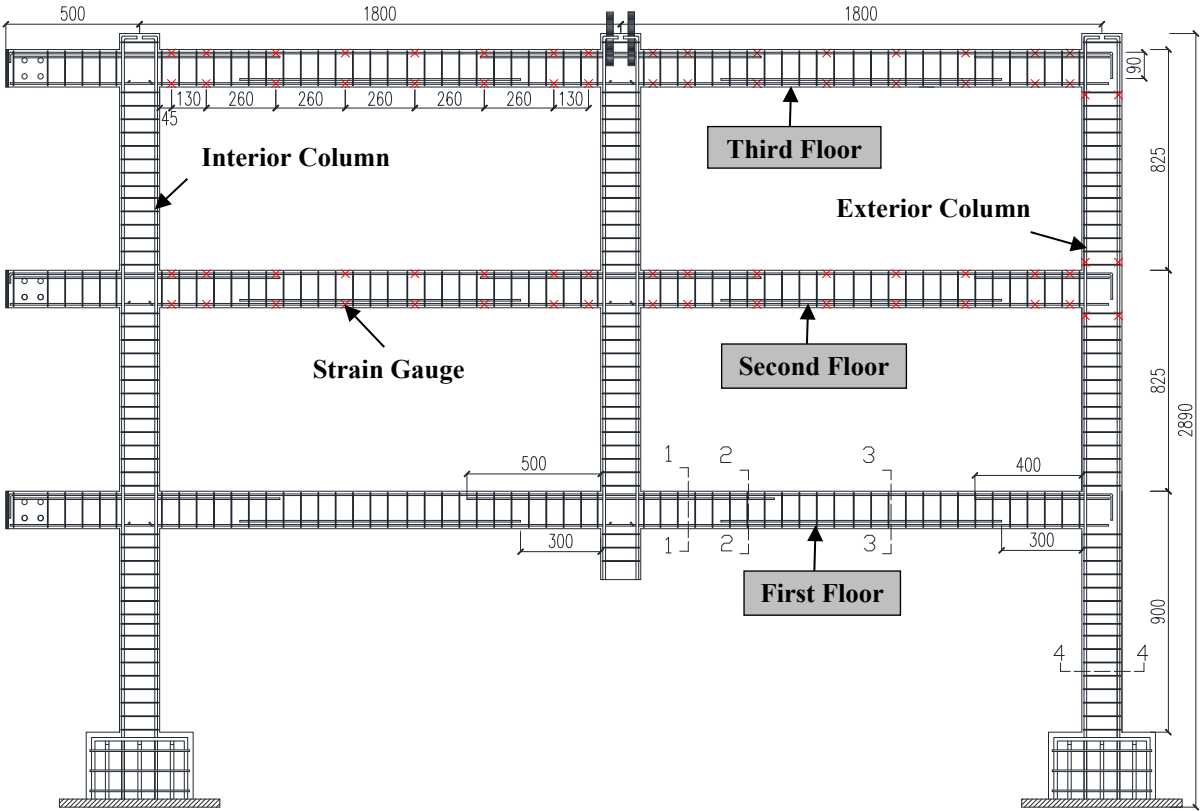
10

11

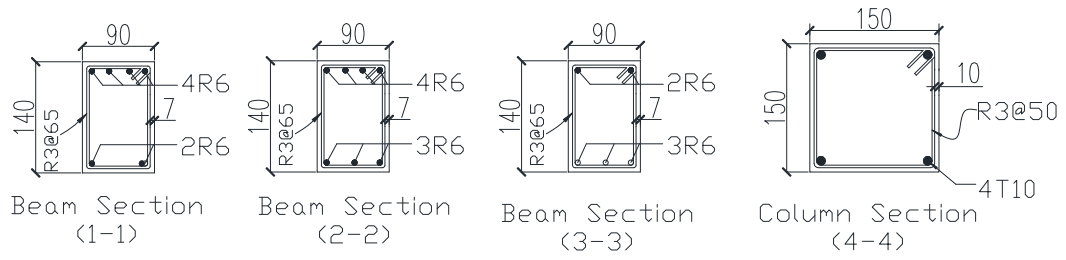
Table 1

Model Parameters of CSCM after Adjustment (Units: N, mm and ms)

| MID     | RO       | NPLOT  | INCRE   | IRATE     | ERODE    | RECOV  | ITRETRC |
|---------|----------|--------|---------|-----------|----------|--------|---------|
| 1       | 0.00232  | 1      | 0.0     | 0         | 1.10     | 0.0    | 0       |
| PRED    |          |        |         |           |          |        |         |
| 0       |          |        |         |           |          |        |         |
| G       | K        | ALPHA  | THETA   | LAMDA     | BETA     | NH     | CH      |
| 7065    | 7738     | 14.788 | 0.3029  | 10.5      | 0.01929  | 0      | 0       |
| ALPHA1  | THETA1   | LAMDA1 | BETA1   | ALPHA2    | THETA2   | LAMDA2 | BETA2   |
| 0.74735 | 0.001102 | 0.17   | 0.06855 | 0.66      | 0.001323 | 0.16   | 0.06855 |
| R       | XD       | W      | D1      | D2        |          |        |         |
| 5.0     | 91.5     | 0.05   | 2.5e-04 | 3.492e-07 |          |        |         |
| B       | GFC      | D      | GFT     | GFS       | PWRC     | PWRT   | PMOD    |
| 100.0   | 4.575    | 0.1    | 0.04575 | 0.02288   | 5.0      | 1.0    | 0.0     |
| ETA0C   | NC       | ETAOT  | NT      | OVERC     | OVERT    | SRATE  | REPOW   |
| 0       | 0        | 0      | 0       | 0         | 0        | 0      | 0       |



(a)



(b)

**Fig. 1**–Reinforcement layout of the Specimen BFS: (a) Elevation view, (b) Cross section of RC frame

Note: Unit in mm, T=Deformed reinforcing bar; R=Plain reinforcing bar

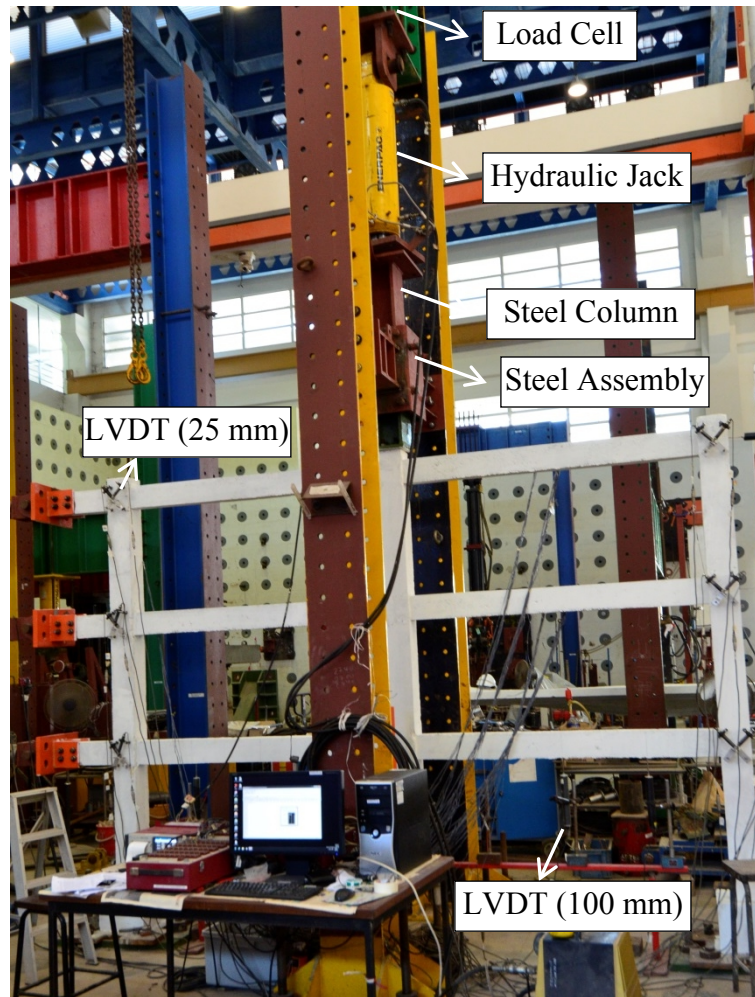


**Fig. 2**–Test setup and instrumentation

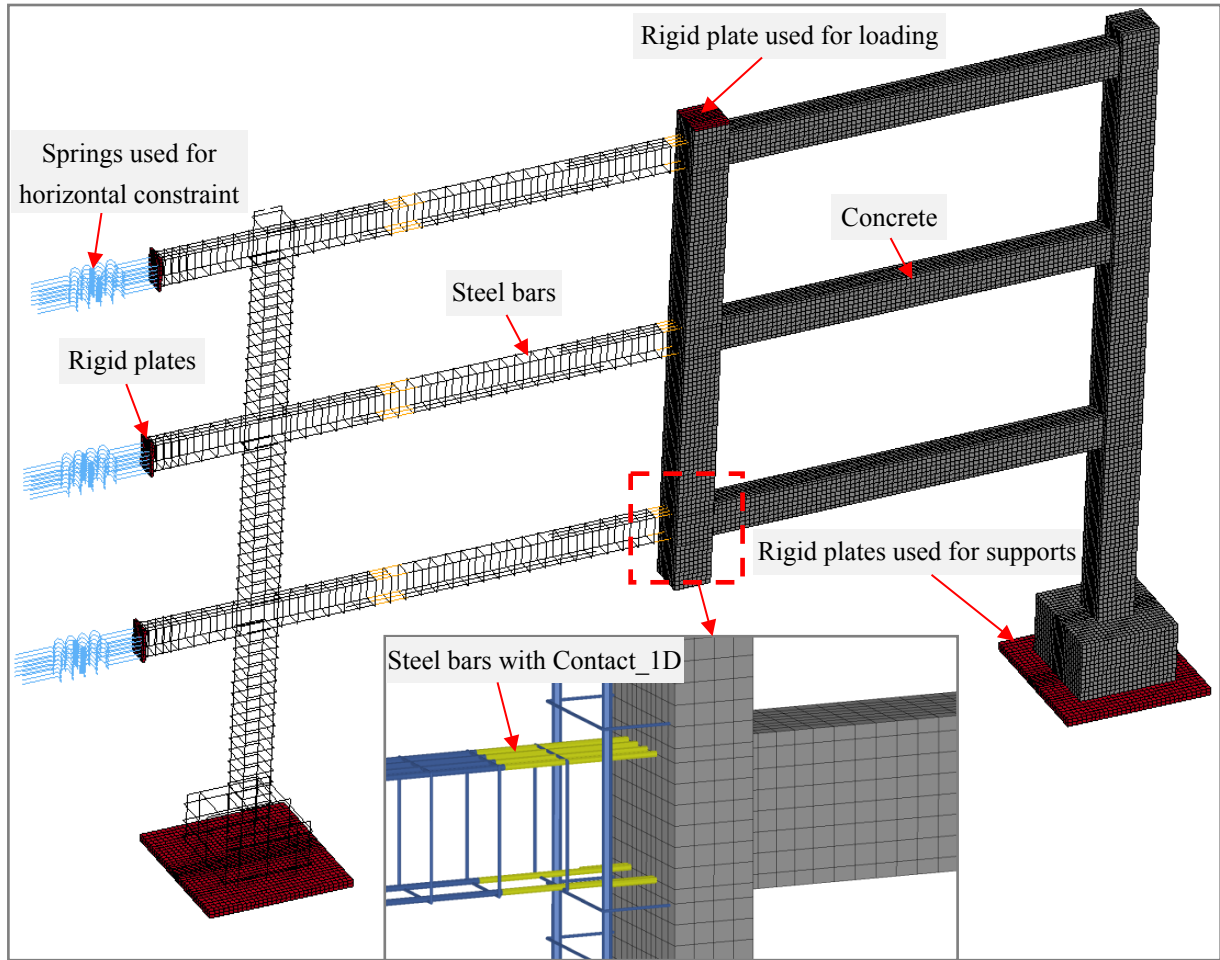


**Fig. 3**—Geometric model of Specimen BFS

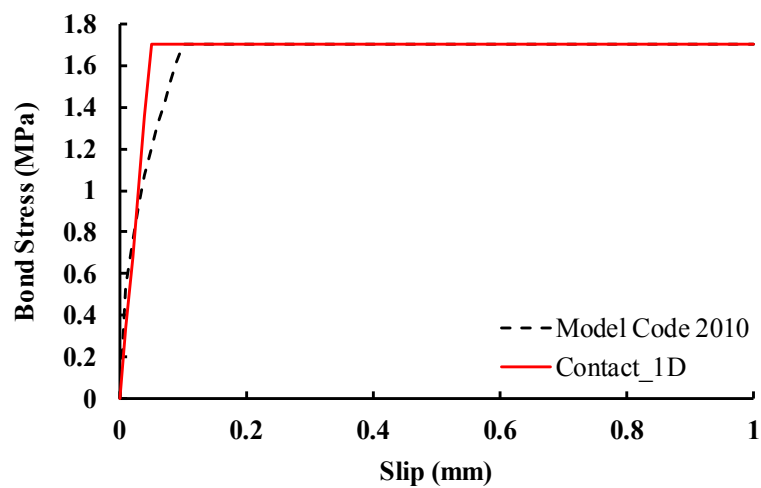


**Fig. 4**—Comparison of bond-slip relationship between Model Code 2010 and Contact\_1D

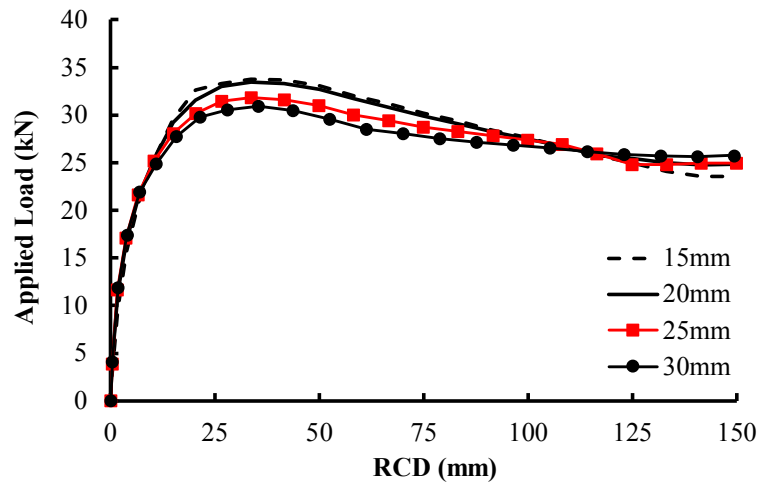


**Fig. 5**–Effects of different mesh sizes

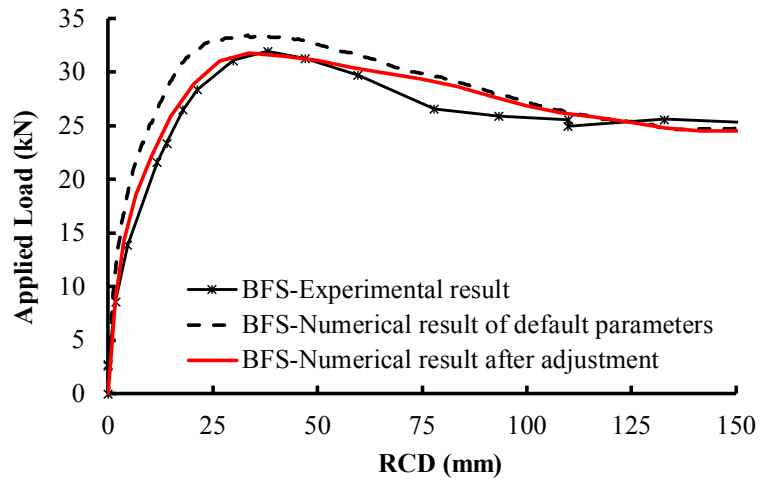


**Fig. 6**–Effects of different concrete input parameters

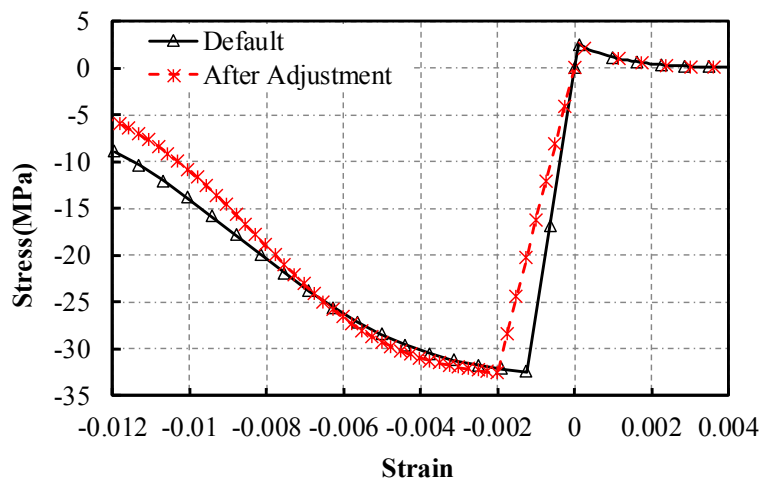
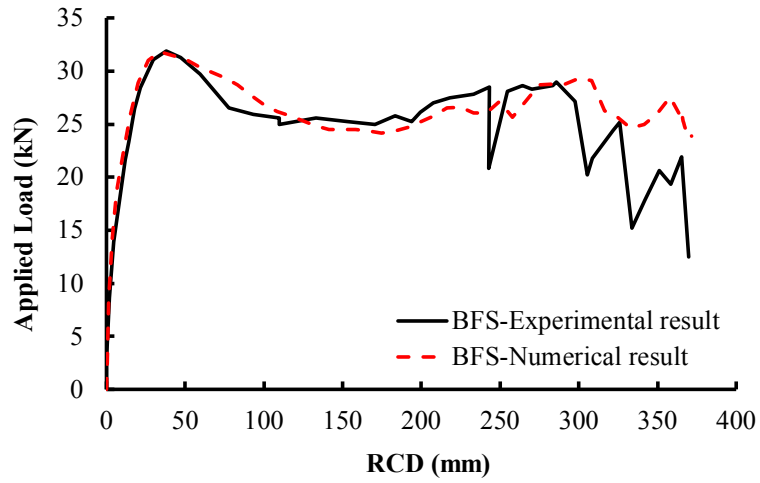
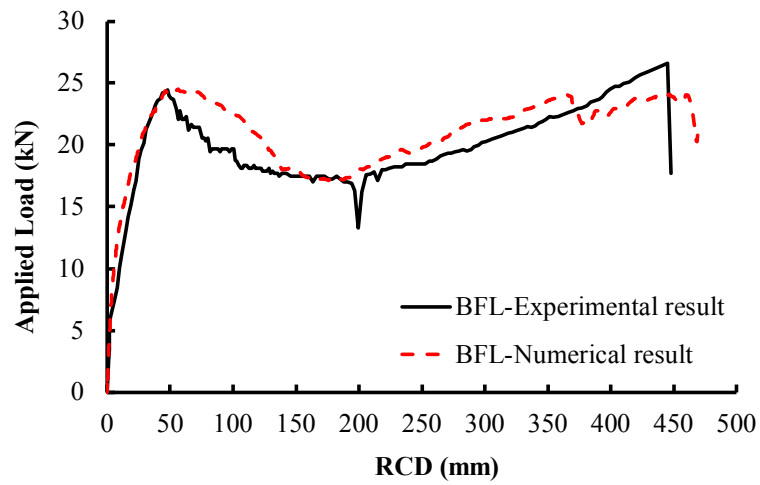


**Fig. 7**–Unconfined uniaxial stress-strain relationship of concrete for 32.1 MPa based on CSCM

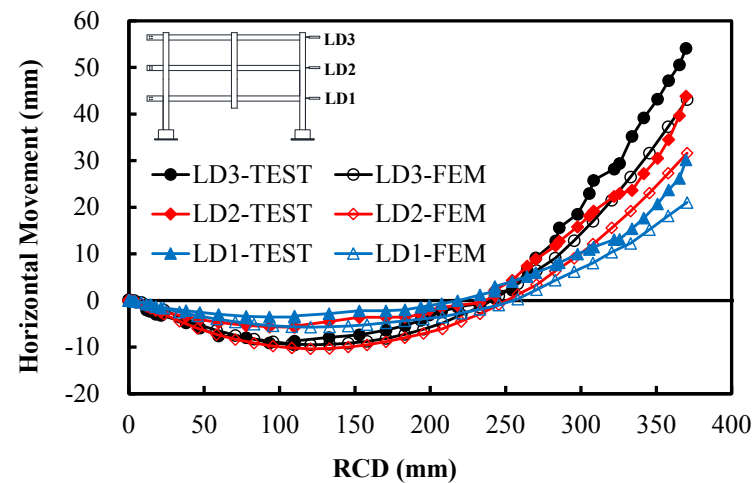


(a)

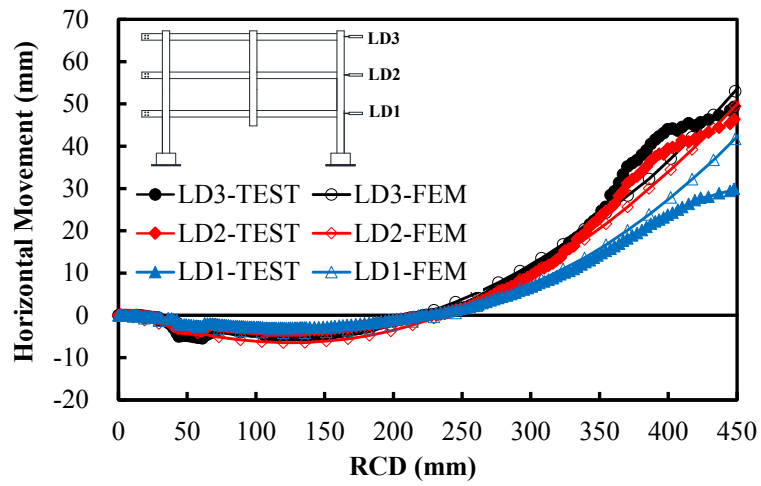


(b)

**Fig. 8**–Comparison of the load-displacement response from numerical and test: (a) BFS, (b) BFL

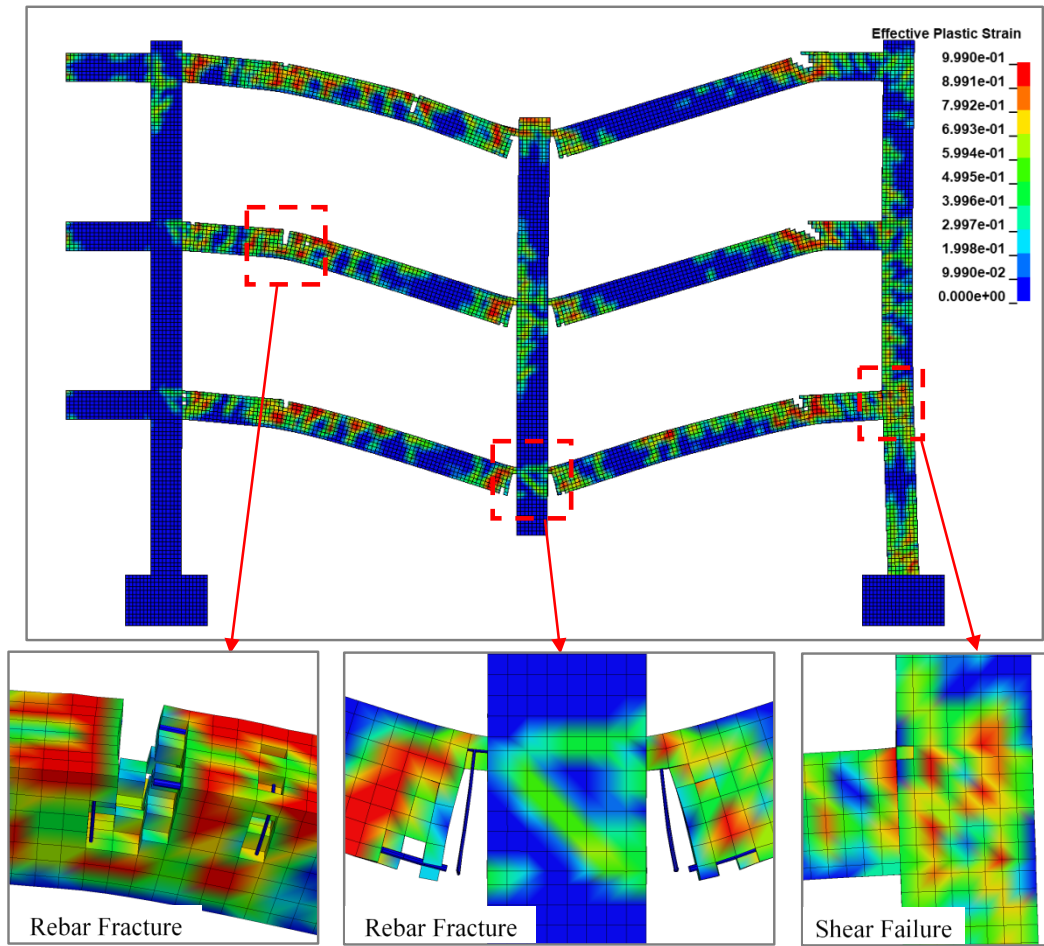


(a)

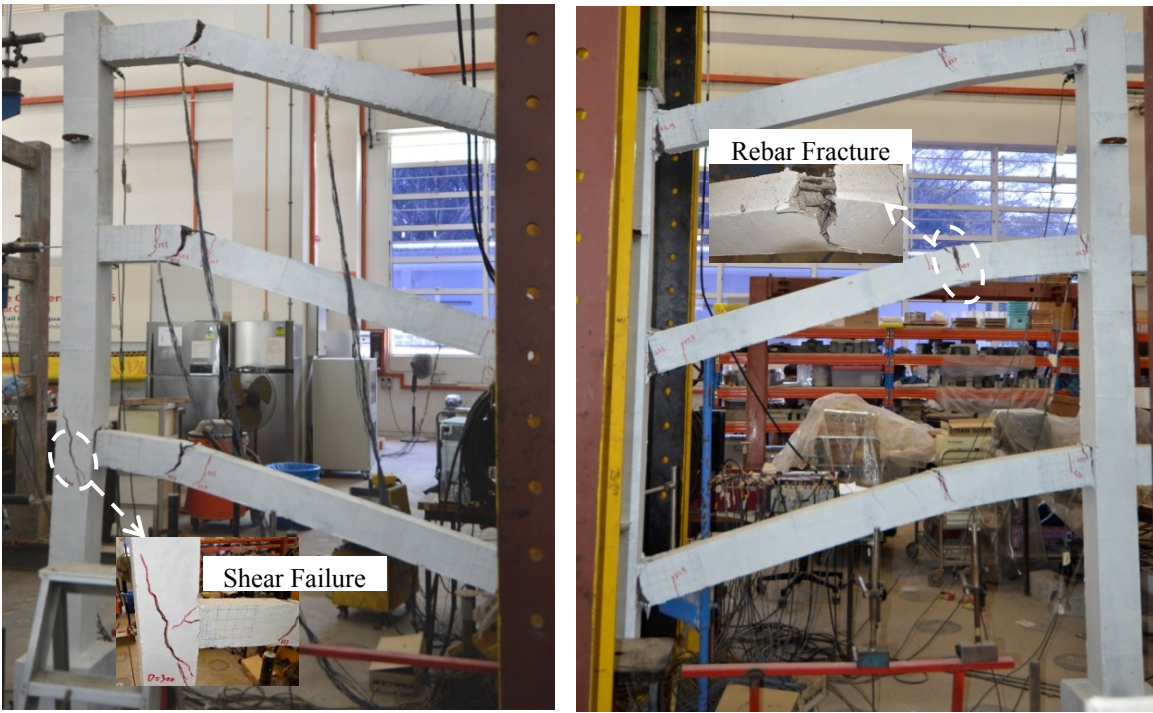


(b)

**Fig. 9**—Comparison of the horizontal movement response from numerical and test: (a) BFS, (b) BFL

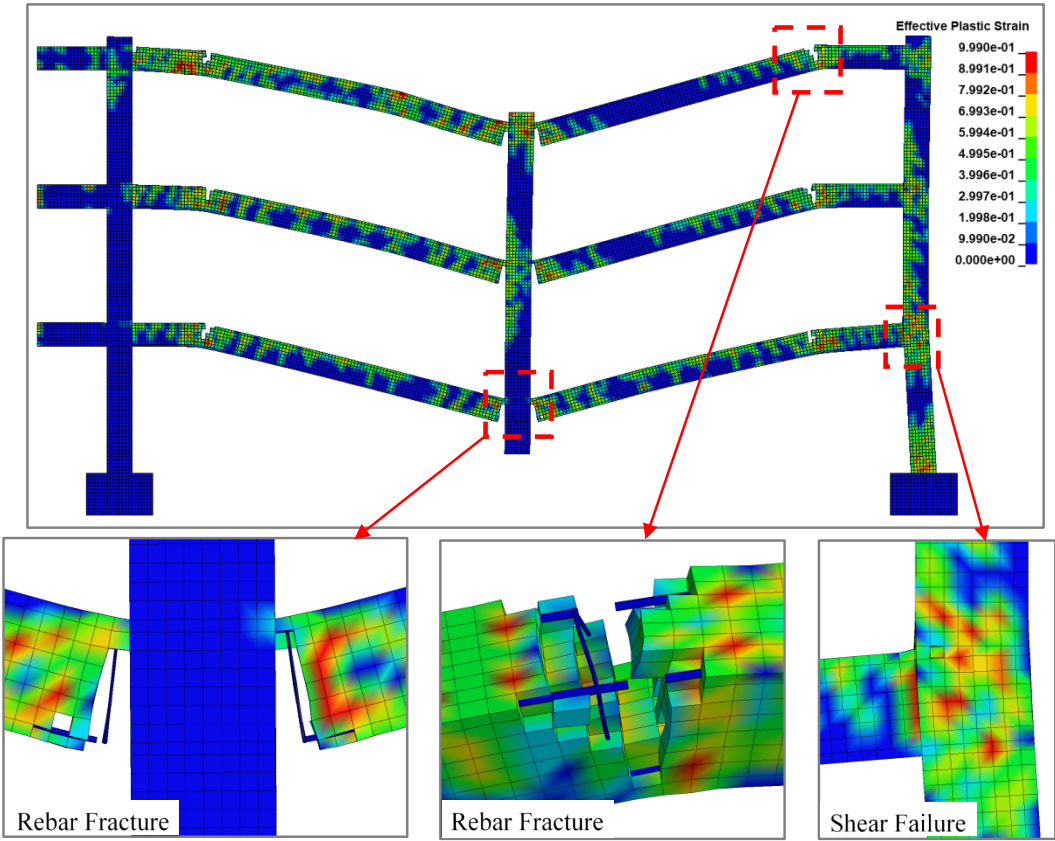


(a)

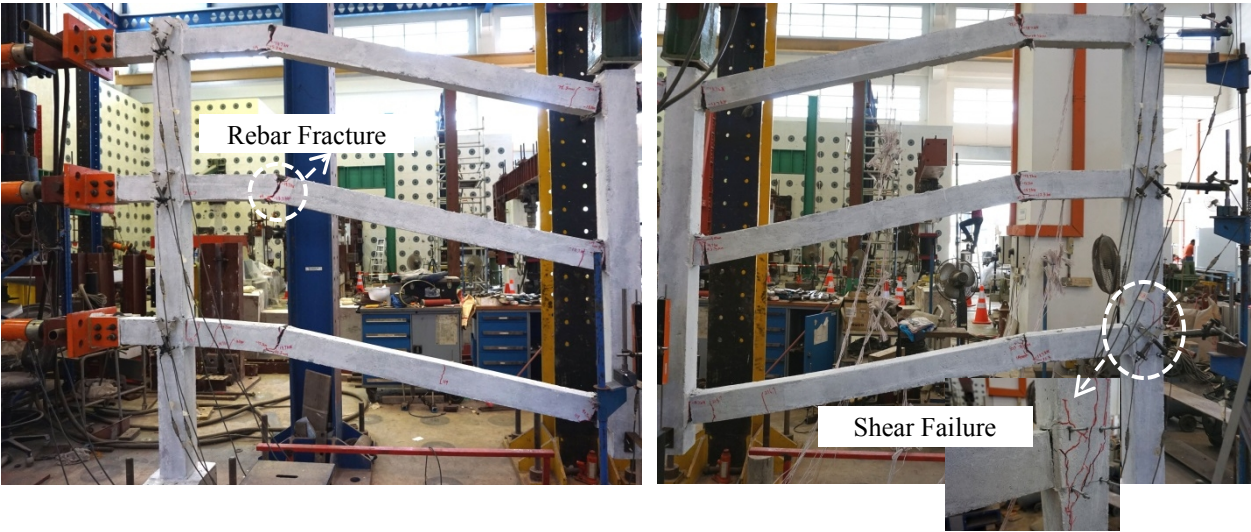


(b)

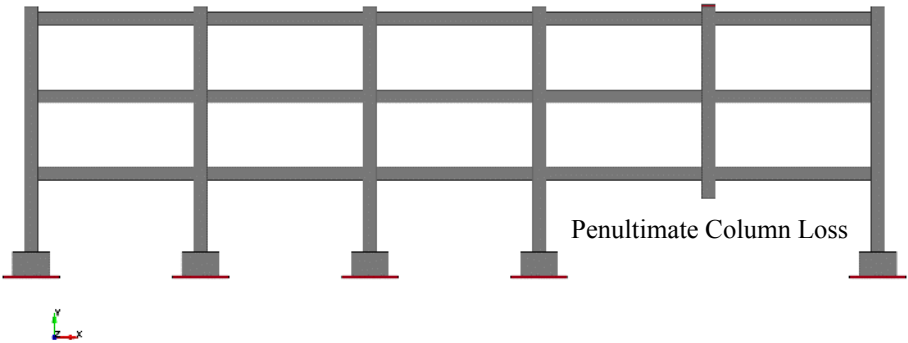
**Fig. 10**—Comparisons of failure mode of BFS: (a) FEM, (b) Test



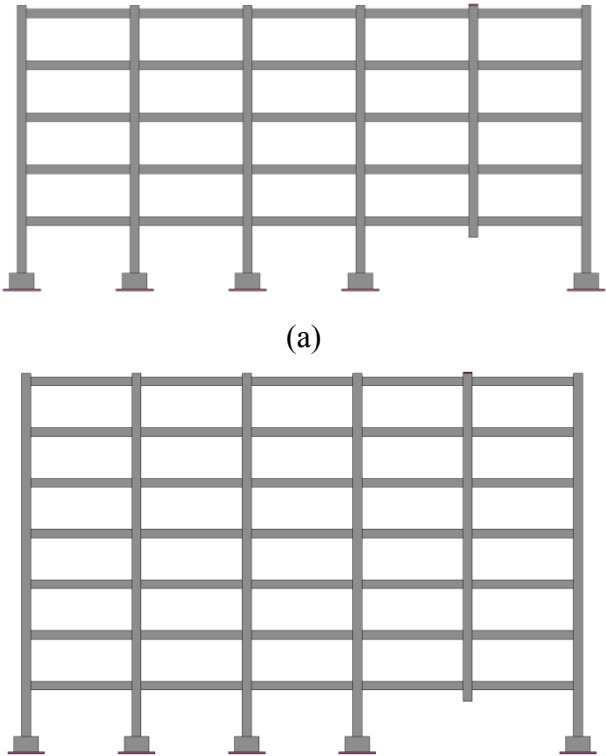
(a)



(b)  
**Fig. 11**–Comparisons of failure mode of BFL: (a) FEM, (b) Test



**Fig. 12**–Numerical model of BFS-P



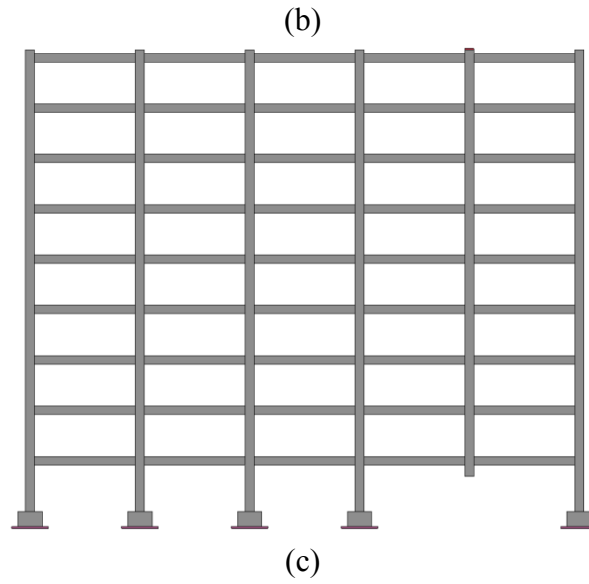


**Fig. 13**–Numerical models of number of different floors: (a) BFS-P-5F, (b) BFS-P-7F, (c) BFS-P-9F

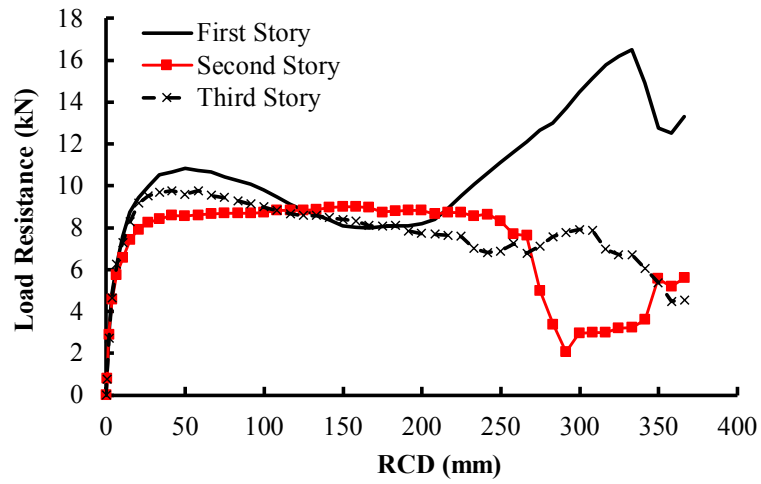


**Fig. 14**–Load resistance of each story of BFS-P

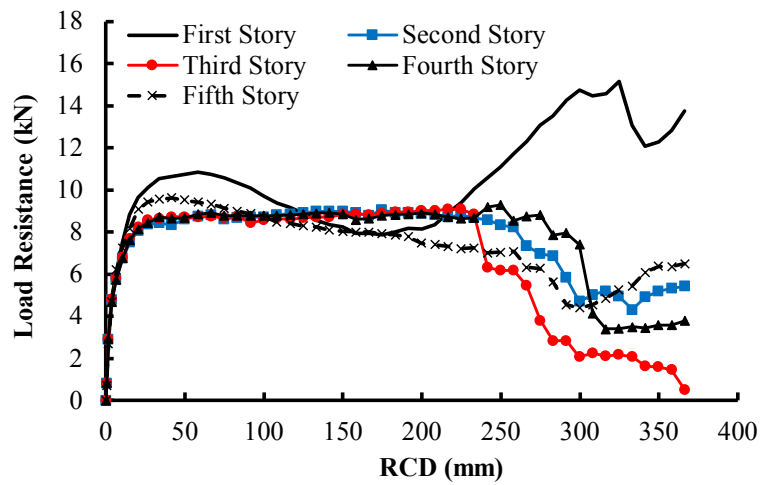


**Fig. 15**–Load resistance of each story of BFS-P-5F

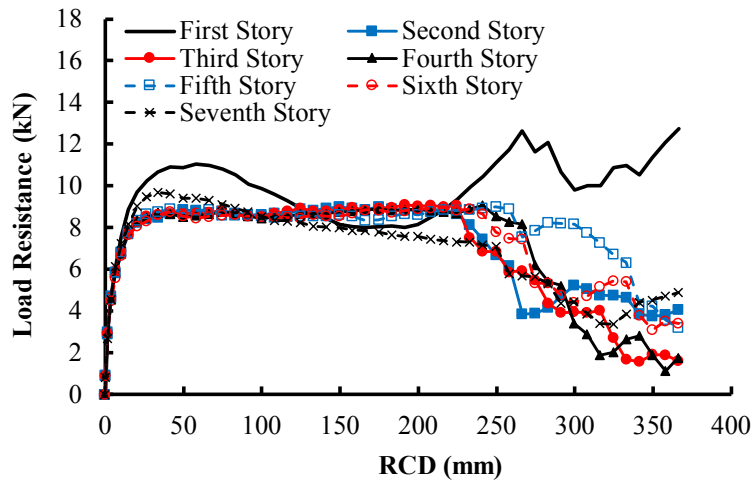


Fig. 16–Load resistance of each story of BFS-P-7F

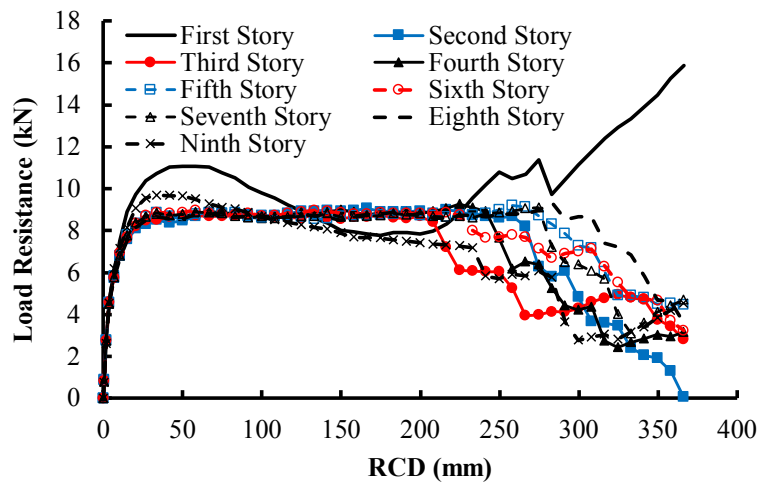
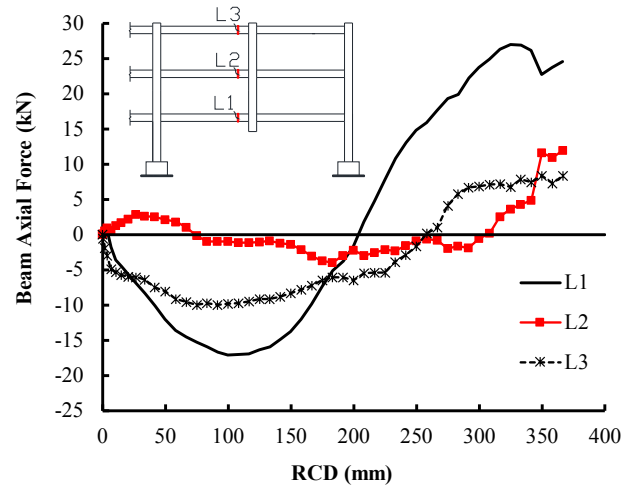
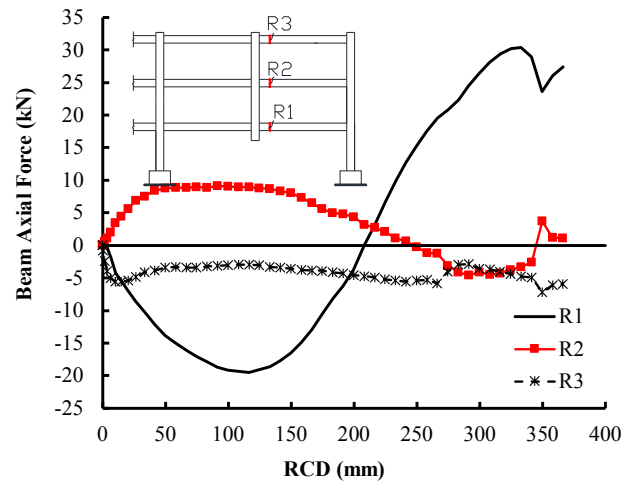


Fig. 17–Load resistance of each story of BFS-P-9F

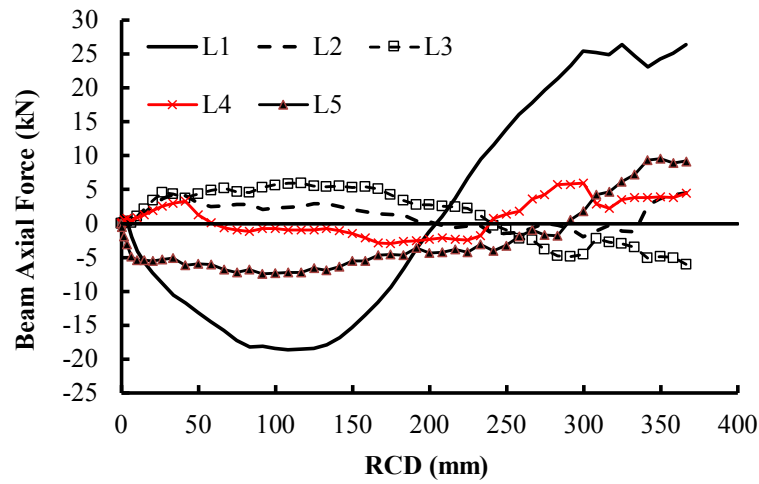


(a)

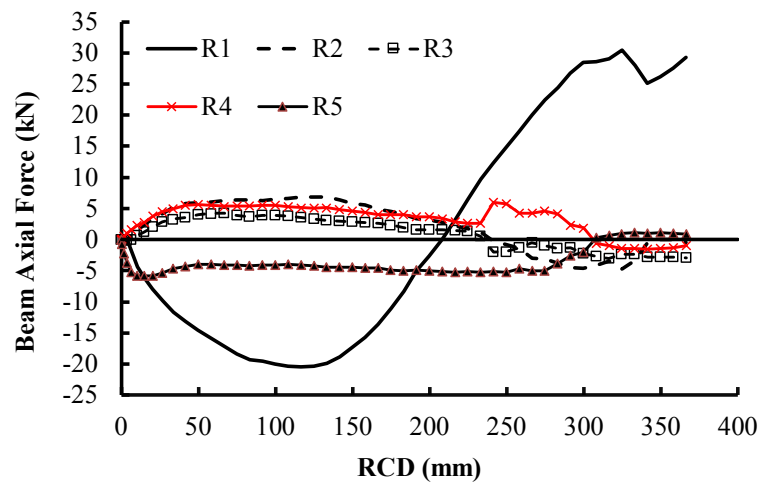


(b)

**Fig. 18**–Varying of beam axial forces of BFS-P: (a) left side of removed column, (b) right side of removed column

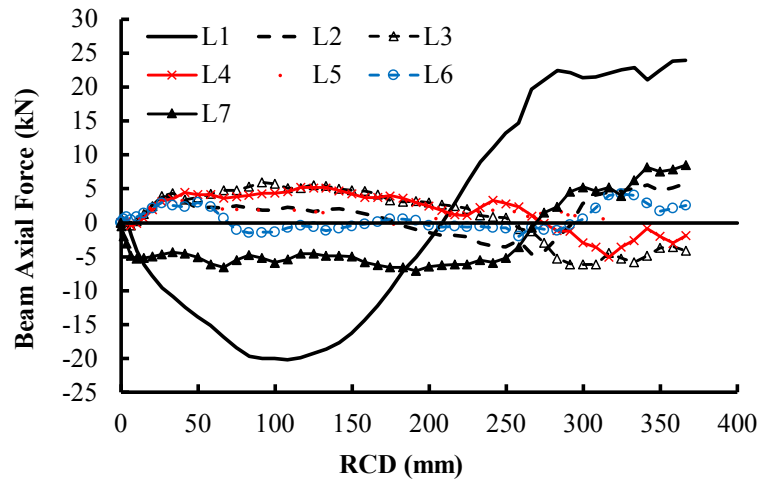


(a)

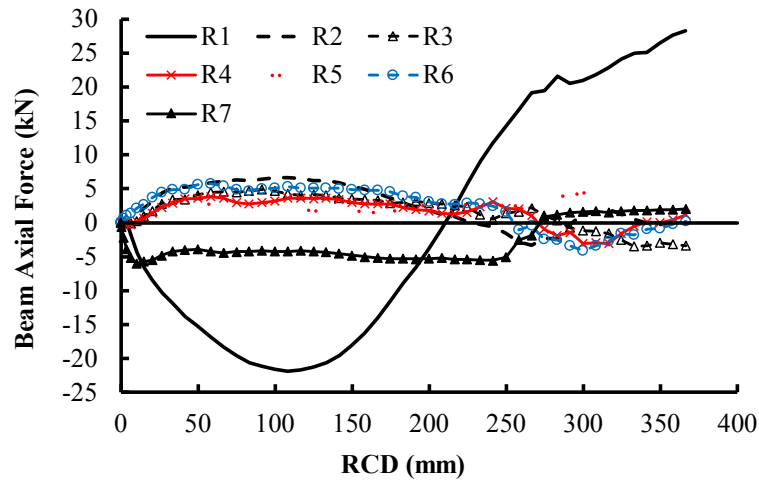


(b)

**Fig. 19**–Varying of beam axial forces of BFS-P-5F: (a) left side of removed column, (b) right side of removed column

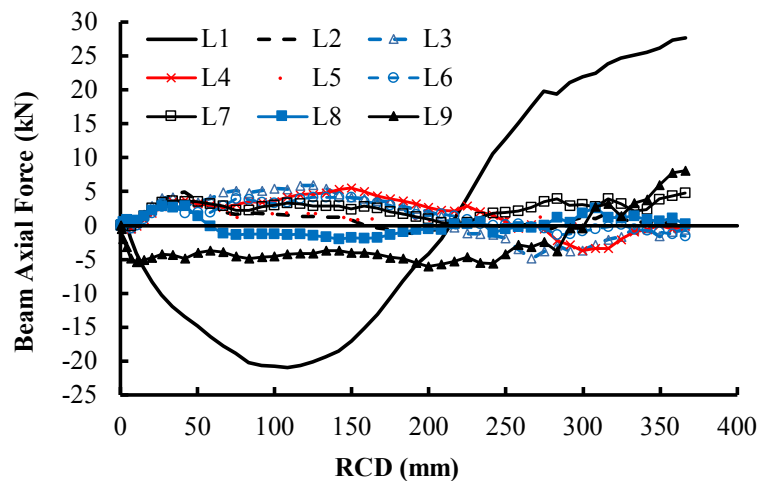


(a)

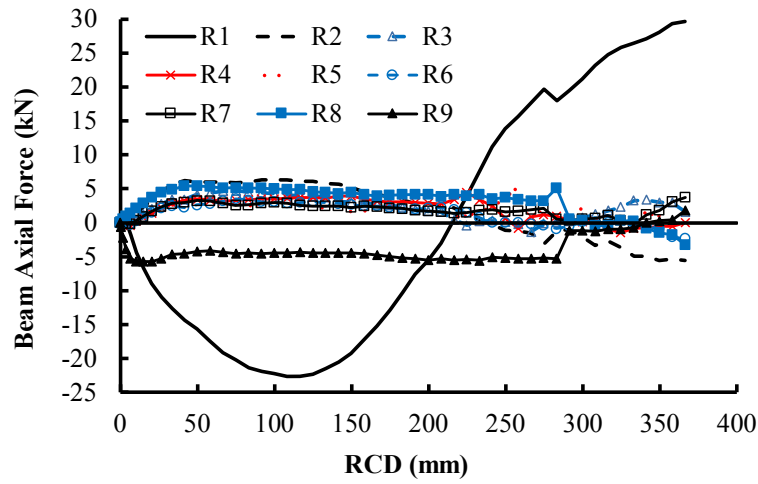


(b)

**Fig. 20**—Varying of beam axial forces of BFS-P-7F: (a) left side of removed column, (b) right side of removed column

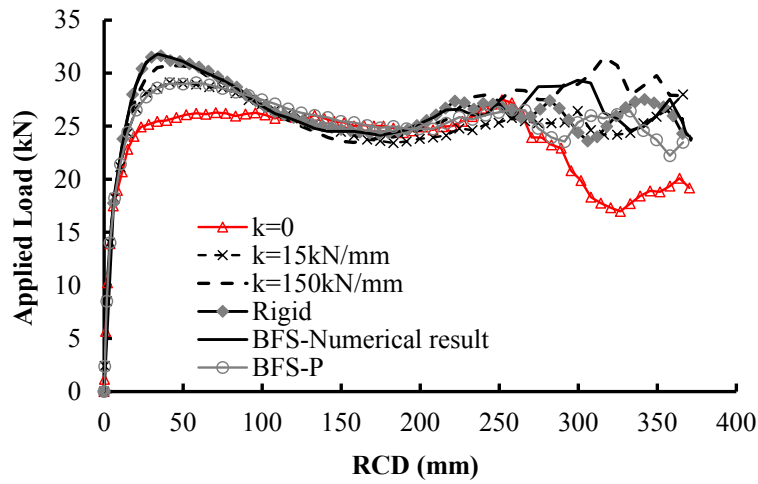


(a)

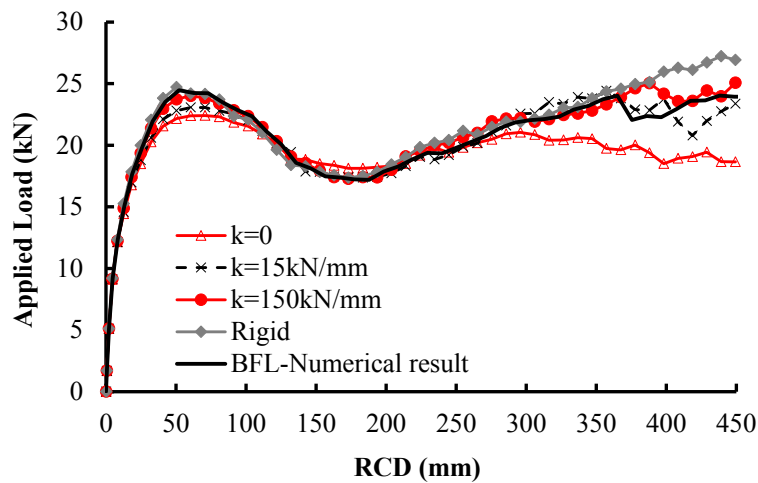


(b)

**Fig. 21**—Varying of beam axial forces of BFS-P-9F: (a) left side of removed column, (b) right side of removed column

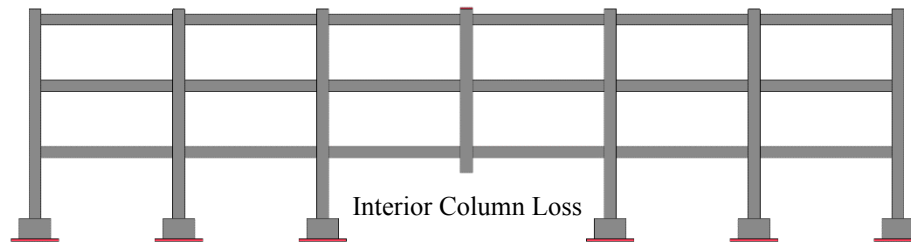


(a)

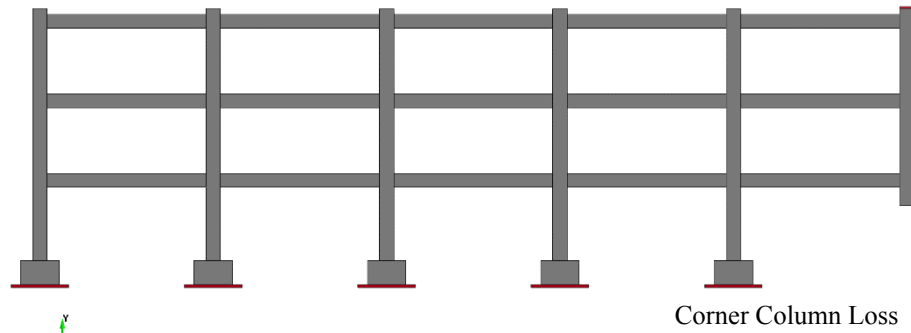


(b)

**Fig. 22**—Effects of horizontal stiffness of the constraints: (a) BFS, (b) BFL



(a)



(b)

**Fig. 23**–Numerical models of different column loss: (a) BFS-I, (b) BFS-C

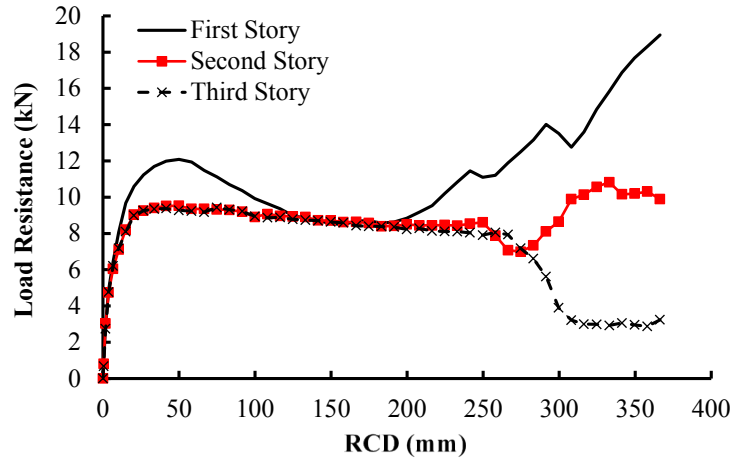


**Fig. 24**–Load resistance of each story of BFS-I

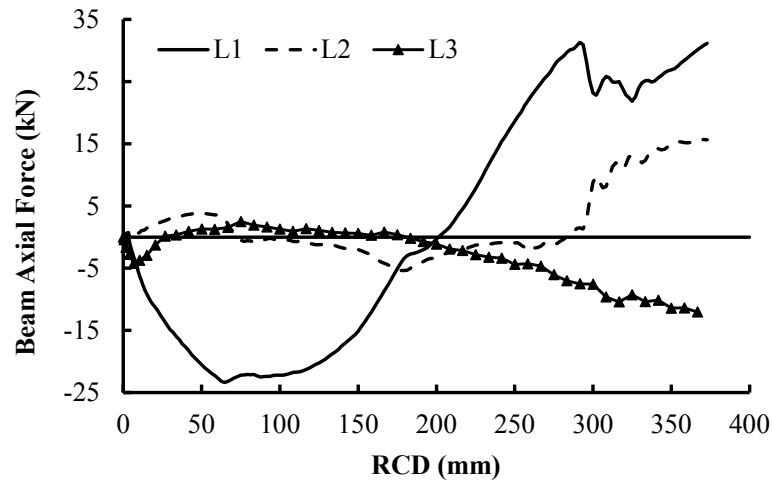


**Fig. 25**–Varying of axial force of the beams in different story of BFS-I

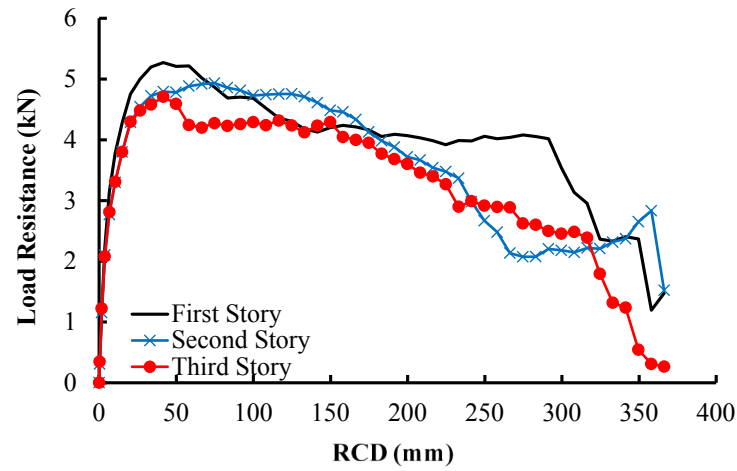


**Fig. 26**–Load resistance of each story of BFS-C